Role of MAO in Chromium-Catalyzed Ethylene Tri- and Tetramerization: A DFT Study

Werner Janse van Rensburg,* Jan-Albert van den Berg, and Petrus J. Steynberg

Sasol Technology (Pty), Ltd., R&D Division, 1 Klasie Havenga Road, Sasolburg 9570, South Africa

Received September 28, 2006

The successful $[Ph_2PN(^iPr)PPh_2]$Cr-catalyzed trimerization and tetramerization of ethylene to 1-hexene and 1-octene requires the presence of a cocatalyst, of which methylaluminoxane (MAO) is particularly relevant. Density functional theory (DFT) calculations are reported on the interaction of various MAO models with chromacycloheptane intermediates. Chromacycloheptanes are well established to be important intermediates during the selective chromium-catalyzed trimerization and tetramerization of ethylene, effectively resembling appropriate models for a study of MAO interaction with chromium complexes during active catalysis. A systematic study is presented evaluating different $(AlOMe)_n$ cage structure models for MAO, as both "classic" MAO cages and cages activated by interaction with trimethylaluminium (TMA), comparing methylation aptitudes of TMA versus MAO models and evaluating the interaction of MAO models with chromacycloheptane intermediates. From the results the importance of the use of realistic ligand and large MAO models is shown to be a prerequisite for obtaining accurate catalyst activation data. In particular, use of a "stripped-down" ligand $[Me_2PN(Me)PMe_2]$ on chromacycloheptane in combination with a relatively small MAO cage $[(AlOMe)_6{\cdot}(AlMe_3)]$ results in the optimization of formally coordinated chromacycloheptane−MAO complexes, even with increased steric congestion on chromium upon coordination of an additional ethylene moiety. In contrast, use of the "full" ligand $[Ph_2PN(^iPr)PPh_2]$ and larger MAO cages $[(AlOMe)_9{\cdot}(AlMe_3)]$ shows that while the formation of formally coordinated chromacycloheptane−MAO complexes are successfully optimized in the absence of additional ethylene, only dissociated ion-pair complexes are present when an additional ethylene molecule is introduced. From these results important insight is gained on the role of MAO during catalysis, as well as the model requirements for both MAO and chromium complexes to conduct fundamental theoretical studies in selective chromium-catalyzed ethylene oligomerization.

Introduction

Among other routes, transition metal-catalyzed oligomerization of ethylene is traditionally used to synthesize α-olefins.[1,2] Although a lot of success has been obtained in developing catalysts that are both stereoselective and highly active, the linear α-olefin products of these technologies usually obey either a Shulz−Flory or Poisson distribution.[3] These distributions of products are due to similar chain propagation and termination rates in the polymerization mechanism proposed by Cossee and Arlman.[4] Consequently, a lot of interest is focused on the development of catalysts capable of selectively producing α-olefins of specific chain lengths. In particular, the selective trimerization of ethylene to 1-hexene is a well-known technology.[5] In addition, it was recently demonstrated that the Cr-catalyzed tetramerization of ethylene can be afforded with up to 70% selectivity.[6,7] In contrast to the Cossee−Arlman mechanism, the high selectivities in ethylene trimerization and tetramerization processes were shown by experiment[8−11] and DFT calculations[12−14] to be a consequence of metallacycle mechanisms.

Transition metal-based oligomerization catalysts generally do not operate alone and must be activated by suitable cocatalysts such as perfluoroaryl boranes, fluoroarylalanes, trityl and

* Corresponding author. E-mail: Werner.JansevanRensburg@sasol.com.

(1) Chen, E.Y.-X.; Marks, T. J. *Chem. Rev.* **2000**, *100*, 1391. (b) Coates, G. W. *J. Chem. Soc., Dalton Trans.* **2002**, *4*, 467. (c) Angermund, K.; Fink, G.; Jensen, V. R., Kleinschmidt, R. *Chem. Rev.* **2000**, *100*, 1457. (d) Coates, G. W. *Chem. Rev.* **2000**, *100*, 1223.

(2) (a) Coates, G. W. *J. Chem. Soc., Dalton Trans.* **2002**, *4*, 467. (b) Angermund, K.; Fink, G.; Jensen, V. R., Kleinschmidt, R. *Chem. Rev.* **2000**, *100*, 1457. (c) Coates, G. W. *Chem. Rev.* **2000**, *100*, 1223.

(3) (a) Flory, P. J. *J. Am. Chem. Soc.* **1940**, *62*, 1561. (b) Schulz, G. V. *Z. Phys. Chem. B* **1935**, *30*, 379. (c) Schulz, G. V. *Z. Phys. Chem. B* **1939**, *43*, 25.

(4) Cossee, P. J. *J. Catal.* **1964**, *3*, 80. (b) Arlman, E. J.; Cossee, P. J. *J. Catal.* **1964**, *3*, 99.

(5) For a comprehensive review on ethylene trimerization see: Dixon, J. T.; Green, M. J.; Hess, F. M.; Morgan, D. H. *J. Organomet. Chem.* **2004**, *689*, 3641.

(6) Bollmann, A.; Blann, K.; Dixon, J. T.; Hess, F. M.; Killian, E.; Maumela, H.; McGuinness, D. S.; Morgan, D. H.; Neveling, A.; Otto, S.; Overett, M. J.; Slawin, A. M. Z.; Wasserscheid, P.; Kuhlmann, S. *J. Am. Chem. Soc.* **2004**, *126*, 14712.

(7) Overett, M. J.; Blann, K.; Bollmann, A.; Dixon, J. T.; Hess, F. M.; Killian, E.; Maumela, H.; Morgan, D. H.; Neveling, A.; Otto, S. *Chem. Commun.* **2005**, 622.

(8) (a) Jolly, P. W. *Acc. Chem. Res.* **1996**, *29*, 544. (b) Emrich, R.; Heinemann, O.; Jolly, P. W.; Kruger, C.; Verhovnik, G. P. J. *Organometallics* **1997**, *16*, 1511.

(9) (a) Briggs, J. R. *J. Chem. Soc., Chem. Commun.* **1989**, 674. (b) Meijboom, N.; Schaveien, C.; Orpen, A. G. *Organometallics* **1990**, *9*, 774.

(10) Agapie, T.; Schofer, S. J.; Labinger, J. A.; Bercaw, J. E. *J. Am. Chem. Soc.* **2004**, *125*, 1304.

(11) Overett, M. J.; Blann, K.; Bollmann, A.; Dixon, J. T.; Haasbroek, D.; Killian, E.; Maumela, H.; McGuinness, D. S.; Morgan, D. H. *J. Am. Chem. Soc.* **2005**, *127*, 10723.

(12) Janse van Rensburg, W.; Grové, C.; Steynberg, J. P.; Stark, K. B.; Huyser, J. J.; Steynberg, P. J. *Organometallics* **2004**, *23*, 1207.

(13) (a) Blok, A. N. J.; Budzelaar, P. H. M.; Gal, A. W. *Organometallics* **2003**, *22*, 2564. (b) de Bruin, T. J. M.; Magna, L.; Raybaud, P.; Toulhoat, H. *Organometallics* **2003**, *22*, 3404. (c) Tobisch, S.; Ziegler, T. *Organometallics* **2003**, *22*, 5392. (d) Tobisch, S.; Ziegler, T. *J. Am. Chem. Soc.* **2004**, *126*, 9059. (e) Tobisch, S.; Ziegler, T. *Organometallics* **2004**, *23*, 4077. (f) Tobisch, S.; Ziegler, T. *Organometallics* **2005**, *24*, 256.

(14) Yu, Z.-X.; Houk, K. N. *Angew. Chem., Int. Ed.* **2003**, *42*, 808.

10.1021/om060890c CCC: $37.00
Publication on Web 01/06/2007

ammonium borate and aluminate salts, aluminum alkyls, and methylaluminoxane (MAO).[1] It is generally accepted that the cocatalyst, among other functions, facilitates alkyl abstraction from the catalyst precursor to yield an anionic cocatalyst fragment [RX^-] and a cationic metal fragment [L_nM^+], which in combination represents the active catalytic system as an ion-pair denoted by [L_nM^+][RX^-].[15] The construction of models for oligomerization catalysts should thus include the cocatalyst; this is evident from the relatively large number of theoretical studies that directly incorporate cocatalysts to represent active catalyst systems for polymerization. In particular, perfluoroaryl borane cocatalysts provide well-characterized ion-pair models for theoretical investigation,[16−18] while ion-pairs involving MAO models as cocatalyst are less prevalent in theoretical studies.[18−22]

In order to obtain accurate theoretical data for the involvement of MAO in catalysis, an accurate theoretical model for MAO is required. However, the structural elucidation of MAO remains a challenge not yet fully resolved. Different structures proposed for the composition of MAO include linear chains, rings, two-dimensional structures, and three-dimensional clusters, all of which represent a possible combination of methylaluminoxane $(-Al(Me)-O-)_n$ units. The direct elucidation of the structure of MAO is plagued by the fact that multiple equilibria are present in MAO solutions, as well as the participation of residual trimethylaluminium (TMA) in the interconversion of various MAO oligomers. Despite these uncertainties, important clues toward the structure of MAO are evident from a number of experimental studies. In particular, the structural determination of alkylaluminoxanes by Barron et al.[23] suggests that MAO of composition $(AlOMe)_n$ has a three-dimensional cage structure in which four-coordinate Al atoms are bridged by three-coordinate oxygen atoms. These results were later confirmed by ^{27}Al NMR data, which showed that n in $(AlOMe)_n$ ranges between 9 and 14 at high temperatures.[24] Examples of these MAO cage structures are summarized in Figure 1.

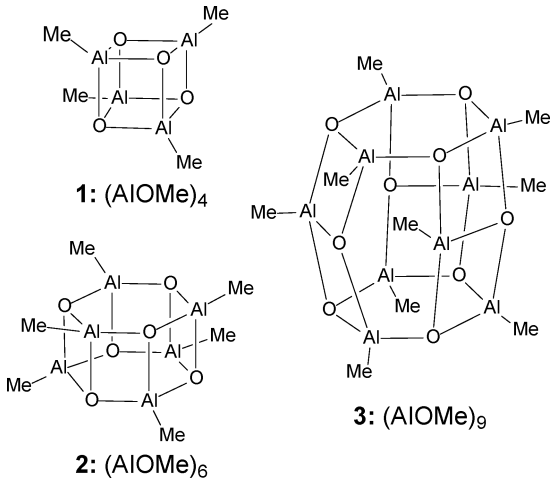

Figure 1. Examples of the cage structures for $(AlOMe)_n$ with n = 4, 6, and 9.

From theoretical studies by Zurek and Ziegler[25,26] it was concluded that MAO models consisting of three-coordinate oxygen and four-coordinate aluminum in three-dimensional cage structures are significantly more stable than linear, ring, or fused ring structures, which is in agreement with the experimental findings of Barron.[23] These $(AlOMe)_n$ cages were found to be the most stable when only square (*s*) and hexagonal (*h*) faces are present, while minimum sterically strained square (*s*) faces are obtained when no octagonal (*o*) faces are present in the cage. It was further pointed out that cages containing square−square (*ss*) edges, i.e., edges where two square−square (*ss*) faces meet, are energetically disfavored, resulting in relatively low abundancy. In accordance with this, it was found that $(AlOMe)_{12}$ is the most abundant MAO cage, explained by the absence of any unfavorable square−square (*ss*) edges in its structure. Comprehensive theoretical studies focusing on similar and alternative MAO cage structures of various sizes were also reported by Zakharov et al.[27,28] and Ystenes et al.[29,30]

"Classic" MAO structures, $(AlOMe)_n$, contain only four-coordinate aluminum centers, which cannot be regarded as being significantly Lewis acidic (Figure 1). It is well known that residual trimethylaluminum (TMA) in MAO is often necessary for MAO to be catalytically active,[31,32] suggesting that the Al:O:Me ratio in MAO is not exactly 1:1:1. This complicates the structural elucidation of MAO, because residual TMA in MAO solutions is suggested to participate in equilibria that interconvert various MAO oligomers.[33,34] Nevertheless, from NMR studies by Imhoff et al.[35] it was shown that the Al, O, and Me composition in MAO corresponds to $(AlO_{0.8-0.75}Me_{1.4-1.5})_n$, effectively suggesting that TMA is incorporated in the structure

(15) Macchioni, A. *Chem. Rev.* **2005**, *105*, 2039.
(16) Lanza, G.; Fragalà, I. L.; Marks, T. J. *Organometallics* **2002**, *21*, 5594.
(17) (a) Vanka, K.; Chan, M. S. W.; Pye, C. C.; Ziegler, T. *Organometallics* **2000**, *19*, 1841. (b) Chan, M. S. W.; Vanka, K.; Pye, C. C.; Ziegler, T. *Organometallics* **1999**, *18*, 4624. (c) Wondimagegn, T.; Xu, Z.; Vanka, K.; Ziegler, T. *Organometallics* **2005**, *24*, 2076. (d) Wondimagegn, T.; Vanka, K.; Xu, Z.; Ziegler, T. *Organometallics* **2004**, *23*, 2651. (e) Vanka, K.; Xu, Z.; Ziegler, T. *Organometallics* **2004**, *23*, 2900. (f) Vanka, K.; Ziegler, T. *Organometallics* **2001**, *20*, 905. (g) Xu, Z.; Vanka, K.; Ziegler, T. *Organometallics* **2004**, *23*, 104. (h) Chan, M. S.W.; Ziegler, T. *Organometallics* **2000**, *19*, 5182. (i) Wondimagegn, T.; Xu, Z.; Vanka, K.; Ziegler, T. *Organometallics* **2004**, *23*, 3847. (j) Vanka, K.; Xu, Z.; Ziegler, T. *Organometallics* **2005**, *24*, 419. (k) Deck, P. A.; Beswick, C. L.; Marks, T. J. *J. Am. Chem. Soc.* **1998**, *120*, 1772. (l) Lanza, G.; Fragalà, I. L.; Marks, T. J. *J. Am. Chem. Soc.* **1998**, *120*, 8257. (m) Lanza, G.; Fragalà, I. L.; Marks, T. J. *J. Am. Chem. Soc.* **2000**, *122*, 12764. (n) Nifant'ev, I. E.; Ustynyuk, L. Y.; Laikov, D. N. *Organometallics* **2001**, *20*, 5375. (o) Nifant'ev, I. E.; Ustynyuk, L. Y.; Besedin, D. V. *Organometallics* **2003**, *22*, 2619.
(18) Xu, Z.; Vanka, K.; Firman, T.; Michalak, A.; Zurek, E.; Zhu, C.; Ziegler, T. *Organometallics* **2002**, *21*, 2444.
(19) (a) Zurek, E.; Zieger, T. *Faraday Disuss.* **2003**, *124*, 93. (b) Zurek, E.; Ziegler, T. *Organometallics* **2002**, *21*, 83.
(20) (a) Belelli, P. G.; Branda, M. M.; Castellani, N. J. *J. Mol. Struct. A: Chem.* **2003**, *192*, 9. (b) Belelli, P. G.; Damiani, D. E.; Castellani, N. J. *J. Mol. Struct. A: Chem.* **2004**, *208*, 147. (c) Belelli, P. G.; Castellani, N. J. *J. Mol. Struct. A: Chem.* **2006**, *253*, 52.
(21) (a) Eilertsen, J. L.; Støvneng, J. A.; Ystenes, M.; Rytter, E. *Inorg. Chem.* **2005**, *44*, 4843. (b) Yang, S. H.; Huh, J.; Jo, W. H. *Macromolecules* **2005**, *38*, 1402. (c) Fusco, R.; Longo, L.; Proto, A.; Masi, F.; Garbassi, F. *Macromol. Rapid. Commun.* **1998**, *19*, 257.
(22) Fusco, R.; Longo, L.; Masi, F.; Garbassi, F. *Macromolecules* **1997**, *30*, 7673.
(23) (a) Mason, M. R.; Smith, J. M.; Bott, S. G.; Barron, A. R. *J. Am. Chem. Soc.* **1993**, *115*, 4971−4984. (b) Harlan, C. J.; Mason, M. R.; Barron, A. R. *Organometallics* **1994**, *13*, 2957−2969.
(24) Babushkin, D. E.; Semikolenova, N. V.; Panchenko, V. N.; Sobolev, A. P., Zakharov, V. A.; Talsi, E. P. *Macromol. Chem. Phys.* **1997**, *198*, 3845−3854.
(25) Zurek, E.; Ziegler, T. *Inorg. Chem.* **2001**, *40*, 3279.
(26) (a) Zurek, E.; Ziegler, T. *Prog. Polym. Sci.* **2004**, *29*, 107. (b) Zurek, E.; Woo, T. K.; Firman, T. K.; Ziegler, T. *Inorg. Chem.* **2001**, *40*, 361.
(27) Zakharov, I. I.; Zakharov, V. A. *Macromol. Theory Simul.* **2001**, *10*, 108.
(28) (a) Zakharov, I. I.; Zakharov, V. A.; Potapov, A. G.; Zhidomirov, G. M. *Macromol. Theory Simul.* **1999**, *8*, 272. (b) Panchenko, V. N.; Zakharov, V. A.; Danilova, I. G.; Paukshtis, E. A.; Zakharov, I. I.; Goncharov, V. G.; Suknev, A. P. *J. Mol. Catal. A* **2001**, *174*, 107.
(29) Ystenes, M.; Eilertsen, J. L.; Liu, J.; Ott, M.; Rytter, E.; Støvneng, J. A. *J. Polym. Sci., Part A: Polym. Chem.* **2000**, *123*, 3106.
(30) Rytter, E.; Støvneng, J. A.; Eilertsen, J. A.; Ystenes, M. *Organometallics* **2001**, *20*, 4466.
(31) Sinn, H. *Macromol. Symp.* **1995**, *97*, 27−52.
(32) Watanabi, M.; McMahon, N.; Harlan, C. J.; Barron, A. R. *Organometallics* **2001**, *20*, 460−467.

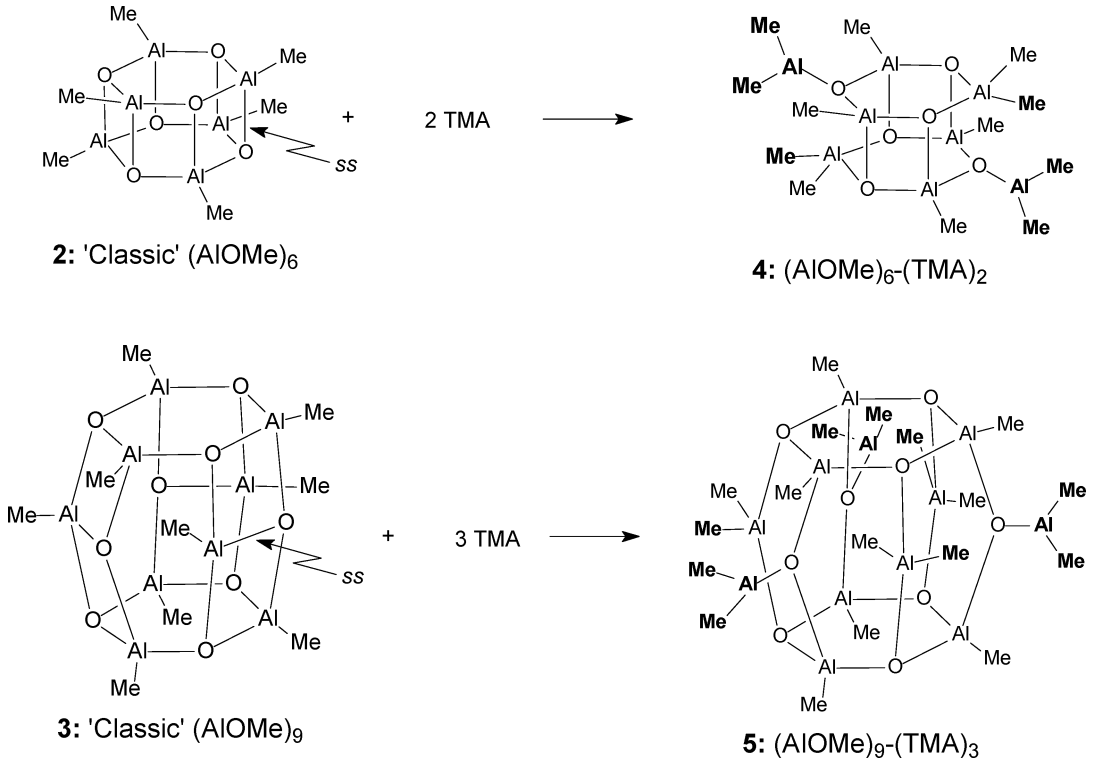

Figure 2. Examples for the transformation of "classic" MAO cages after interaction with TMA.

of "classic" MAO. This led Zhakharov and Zakharov[27] to construct models for what the authors referred to as "true" MAO in their DFT studies by incorporating TMA into "classic" MAO $(AlOMe)_n$ according to the following general reaction:

$$(AlOMe)_n + n/3\ TMA \rightarrow (AlO_{0.75}Me_{1.5})_{n+n/3} \qquad (1)$$

Figure 2 illustrates the mechanism for incorporation of TMA in the MAO cage: it involves the cleavage of an *ss* Al−O bond in the "classic" MAO cage with concerted cleavage of an Al−Me in TMA followed by concurrent formation of new Al−Me and O−Al$(CH_3)_2$ bonds in MAO. It is significant to note that the ratio of acidic three-coordinate Al atoms to four-coordinate Al atoms is significantly higher in experimentally investigated MAO structures compared to "classic" model MAO cages, in agreement with ^{27}Al NMR characterization of MAO, which showed that while four-coordinate Al sites predominate in MAO solutions,[36] three-coordinate sites are also present.[37,38]

However, calculations performed by Zurek and Ziegler[25] indicated that incorporation of TMA into "classic" MAO to yield a Me:Al ratio of 1.5 is energetically unfavorable, effectively suggesting that less TMA should be present. In addition, it was shown that for all "classic" MAO cage structures, except for $(AlOMe)_9$ (vide infra), the incorporation of TMA leads to cleavage of the most reactive square−square (*ss*) Al−O bond, as illustrated in Figure 2. The relief of the square−square ring strain was thus proposed to account for the fact that TMA does indeed incorporate into the "classic" MAO cages.

It is the purpose of the current study to gain fundamental understanding of the role of MAO as cocatalyst for Cr-catalyzed trimerization and tetramerization of ethylene via application of DFT calculations. Whereas a number of theoretical studies have been reported that focus on cocatalyst interaction with transition metal catalysts, and the influence this has on the ethylene polymerization mechanism, no such studies are, to the best of our knowledge, available for Cr catalysts in general and ethylene trimerization/tetramerization systems in particular. A systematic study of the interaction of different MAO models to suitable chromacycloheptane complexes, believed to be active intermediates in a metallacycle mechanistic sequence, is presented.

Computational Details

All geometry optimizations were performed with the DMol^3 density functional theory (DFT) code[39] as implemented in the MaterialsStudio (Version 3.2) program available from Accelrys Inc. Two nonlocal generalized gradient approximation (GGA) exchange−correlation functionals were employed in the current study, viz., the PW91 functional of Perdew and Wang[40] and the revised PBE functional of Hammer, Hanson, and Nørskov[41] (termed RPBE). These functionals were employed for different applications as explicitly noted in the text. DMol^3 utilizes a basis set of numeric atomic functions, which are exact solutions to the Kohn−Sham equations for the atoms.[42] These basis sets are generally more complete than a comparable set of linearly independent Gaussian functions and have been demonstrated to have small basis set

(33) Resconi, L.; Bossi, S.; Abis, L. *Macromolecules* **1990**, *23*, 4489.
(34) (a) Pasynkiewics, S. *Polyhedron* **1990**, *9*, 429. (b) Gianetti, E.; Nicoletti, G.; Mazzochi, R. *J. Polym. Sci., Polym. Chem. Ed.* **1985**, *23*, 2117.
(35) Imhoff, D. W.; Simeral, L. S.; Sangokoya, S. A.; Peel, J. H. *Organometallics* **1998**, *17*, 1941−1945.
(36) Sugano, T.; Matsubara, K.; Fujita, T.; Takahashi, T. *J. Mol. Catal.* **1993**, *82*, 93.
(37) Siedle, A. R.; Lamanna, W. M.; Newmark, R. A.; Stevens, J.; Richardson, D. E.; Ryan, M. *Macromol. Symp.* **1993**, *66*, 215.
(38) Siedle, A. R.; Newmark, R. A.; Lamanna, W. M.; Schroepfer, J. N.; *Polyhedron* **1990**, *9*, 301.
(39) (a) Delley, B. *J. Chem. Phys.* **1992**, *92*, 508. (b) Delley, B. *J. Phys. Chem.* **1996**, *100*, 6107. (c) Delley, B. *J. Chem. Phys.* **2000**, *113*, 7756.
(40) Perdew, J. P.; Wang, Y. *Phys. Rev. B* **1992**, *45*, 13244.
(41) Hammer, B.; Hansen, L. B.; Nørskov, J. K. *Phys. Rev. B* **1999**, *59*, 7413.
(42) Delley, B In *Modern Density Functional Theory: A Tool for Chemistry*; Seminario, J. M., Politzer, P., Eds.; Theoretical and Computational Chemistry, Vol. 2; Elsevier: Amsterdam, The Netherlands, 1995.

superposition errors.[42] In the present study an all-electron polarized split valence basis set, termed double numeric polarized (DNP), has been used. All geometry optimizations employed highly efficient delocalized internal coordinates.[43] The use of delocalized coordinates significantly reduces the number of geometry optimization iterations needed to optimize larger molecules compared to the use of traditional Cartesian coordinates. The tolerance for convergence of the SCF density was set to 10^{-5} hartrees, while the tolerance for energy convergence was set to 2×10^{-6} hartrees. Additional convergence criteria include the tolerance for converged gradient (4×10^{-4} hartrees/Å) and the tolerance for converged atom displacement (5×10^{-4} Å). For all calculations involving chromium the SCF convergence was improved by allowing for fractional electron occupation numbers of near-vacuum energy levels by calculating a finite-temperature Fermi function. A thermal smearing of 5×10^{-3} hartrees was used throughout. In selected cases optimized geometries were subjected to full numerical vibrational analyses at the same level of theory to characterize the nature of equilibrium structures. All calculations were performed without the incorporation of solvent effects, motivated by the fact that Cr-PNP-catalyzed ethylene trimerization/tetramerization is commonly performed in nonpolar solvents such as toluene and cyclohexane. Population analysis (Hirshfeld charges)[44] was performed for selected GGA/RPBE/DNP-optimized structures at the same level of theory.

A comprehensive spin state validation and analysis was performed to establish the ground spin states of Cr(III) complexes. The details of this validation study are included in the Supporting Information. It was found that the RPBE exchange−correlation functional provides particularly accurate relative energies for different spin states of Cr(III) complexes. Quartet (S_3) spin states were calculated to be consistently lower in energy compared to the corresponding doublet (S_1) spin states for all the Cr(III) complexes considered, effectively favoring a quartet (S_3) ground state. This is in agreement with other theoretical studies that also showed that high-spin ground states are favored for chromium complexes with oxidation states 2−4.[12,45] In addition, magnetic susceptibility studies showed that a quartet (S_3) spin state represents the ground state for Cr(III) complexes.[46]

Table 1. Comparative Calculated and Experimental TMA Dimerization Energies (kcal/mol) and Dimer Al−Al Distance (in Å)

method	basis	ΔE	ΔH	ΔG	$T\Delta S$	R(Al−Al)
Present Work						
DMol^3/PW91	DNP	−18.4	−15.9	−3.2	−12.8	2.624
DMol^3/RPBE	DNP	−11.4	−8.6	5.3	−13.8	2.643
Previous Work						
BP86[a]	DZP			0.4		
DPW91[b]	DZP	−12.0	−9.5	7.5	−17.0	2.642
BLYP[c]	6-31G*	−6.1	−2.4	8.7	−10.1	2.638
MP2[c]	Pol. SBK	−21.8	−18.1	−7.0	−11.1	2.587
MP2[c]	6-31G*	−24.6	−20.9	−9.8	−11.1	2.595
MP2[d]	6-31G**	−20.0	−17.4			2.60
DMol/LDA/VWN[e]	DN	−19.8				
DMol/NLDA/PWB[e]	DN	−7.9				
Experiment						
			−20.4[f]	−7.6[f]	−12.8[f]	2.619[g]
						2.606[h]
						2.700[i]

[a] Ref 25. [b] Ref 29. [c] Ref 48. [d] Ref 49. [e] Ref 22. [f] Ref 47. [g] Gas-phase electron diffraction, $T = 333$ K, ref 50. [h] X-ray diffraction, $T = 103$ K, ref 60. [i] Neutron diffraction, $T = 4.5$ K, ref 61.

Results

The presentation of results is divided into four main focus areas, i.e., the conversion of "classic" MAO models to TMA-expanded MAO models, the methylation aptitude of MAO versus TMA, analysis of chromacycloheptane models in the absence of MAO, and the interaction of MAO models with chromacycloheptane models.

"Classic" MAO versus TMA-Expanded MAO. TMA exists as a dimer [$Al_2(CH_3)_4$, **6**],[60,61] which requires the dissociation of a monomeric TMA unit from the dimer before interaction with MAO can proceed. The calculated dimerization enthalpy ($\Delta H_{298.15K}$) of TMA (PW91) is −15.9 kcal/mol, in fair agreement with the experimentally determined dimerization enthalpy of −20.4 kcal/mol at 298.15 K.[47] The DMol^3/PW91-calculated dimerization enthalpy, entropy, and Gibbs free energy are summarized in Table 1 for comparison with DMol^3/RPBE data, previously published calculated data, and experimental data. Table 1 shows that the DMol^3/PW91 calculations represent the

(43) Andzelm, J.; King-Smith, R. D.; Fitzgerald, G. *Chem. Phys. Lett.* **2001**, *335*, 321.
(44) (a) Hirshfeld, F. L. *Theor. Chim. Acta B* **1977**, *44*, 129. (b) Wiberg, K. B.; Rablen, P. R. *J. Comput. Chem.* **1993**, *1412*, 1504.
(45) (a) Cohen, R.; Weitz, E.; Martin, J. M. L.; Ratner, M. A. *Organometallics* **2004**, *23*, 2315. (b) Collagne, E.; Duret, D.; Poli, R. *Dalton Trans.* **1999**, 875. (c) Cacelli, I.; Keogh, D. W.; Poli, R.; Rizzo, A. *New J. Chem.* **1997**, *21*, 133. (d) Hess, J. S.; Leelasubcharoen, S.; Rheingold, A. L.; Doren, D. J.; Theopold, K. H. *J. Am. Chem. Soc.* **2002**, *124*, 2454. (e) Hoganson, C. W.; Doren, D. J.; Theopold, K. H. *Macromolecules* **2004**, *37*, 566.
(46) (a) Carney, M. J.; Robertson, N. J.; Halfen, J. A.; Zakharov, L. N.; Rheingold, A. L. *Organometallics* **2004**, *23*, 6184−6190. (b) Ganesan, M.; Gabbaï, F. P. *Organometallics* **2004**, *23*, 4608−4613. (c) Agapie, T.; Day, M. W.; Henling, L. M.; Labinger, J. A.; Bercaw, J. E. *Organometallics* **2006**, *25*, 2733. (d) Schofer, S. J.; Day, M. W.; Henling, L. M.; Labinger, J. A.; Bercaw, J. E. *Organometallics* **2006**, *25*, 2743.
(47) Smith, M. B. *J. Organomet. Chem.* **1972**, *46*, 31.
(48) Tosell, J. A. *Oragnometallics* **2002**, *21*, 4523−4527.
(49) Kaminsky, W.; Steiger, R. *Polyhedron* **1988**, *7*, 2375.
(50) Cam, D.; Giannini, U. *Makromol. Chem.* **1992**, *193*, 1049.
(51) (a) Gassman, P. G.; Callstrom, M. R. *J. Am. Chem. Soc.* **1987**, *109*, 7875. (b) Sishta, C.; Hathorn, R. M.; Marks, T. J. *J. Am. Chem. Soc.* **1992**, *114*, 1112. (c) Siedle, A. R.; Lamanna, W. M.; Newmark, R. A.; Schroepfer, J. N. *J. Mol. Catal.* **1998**, *128*, 257. (d) Tritto, I.; Li, S. X.; Sacchi, M. C.; Locatelli, P.; Zannoni, G. *Macromolecules* **1995**, *28*, 5358. (e) Tritto, I.; Li, S. X.; Sacchi, M. C.; Zannoni, G. *Macromolecules* **1993**, *26*, 7111. (f) Kaminsky, W. *Makromol. Chem. Phys.* **1996**, *197*, 3907. (g) Kaminsky, W.; Strubel, C. *J. Mol. Catal.* **1998**, *128*, 191. (h) Bryliakov, K. P.; Babushkin, D. E.; Talsi, E. P.; Voskoboynikov, A. Z.; Gritzo, H.; Schröder, L.; Damrau, H.-R. H.; Wieser, U.; Schaper, F.; Brintzinger, H. H. *Organometallics* **2005**, *24*, 894. (i) Castro, P. M.; Lahtinen, P.; Axenov, K.; Viidanoja, J.; Kotiaho, T.; Leskelä, M.; Repo, T. *Organometallics* **2005**, *24*, 3664.
(52) See Supporting Information for an analysis and validation of DFT-calculated spin state splittings for chromium complexes.
(53) Harvey, J. N. *Struct. Bonding* **2004**, *112*, 151−184.
(54) Rappé, A. K.; Skiff, W. M.; Casewit, C. J. *Chem. Rev.* **2000**, *100*, 1435.
(55) Blann, K.; Bollmann, A.; Dixon, J. T.; Hess, F. M.; Killian, E.; Maumela, H.; Morgan, D. H.; Neveling, A.; Otto, S.; Overett, M. *Chem. Commun.* **2005**, 620.
(56) As pointed out by a referee, it could be argued that the size of the MAO model may not necessarily be the driving force for dissociated ion-pair formation, but rather the nature of the ligand. However, calculations performed on interaction of chromacycloheptane complexes containing the "full" $Ph_2PN(^iPr)PPh_2$ ligand and the small TMA-expanded MAO model, $(AlOMe)_6$−TMA, showed that spontaneous ion-pair formation does not occur, even in the presence of an additional coordinating ethylene unit. Alternatively, calculation of complexes containing the "stripped-down" ligand, $Me_2PN(Me)PMe_2$, and the larger TMA-expanded MAO, $(AlOMe)_9$−TMA-*sh*, also resulted in no spontaneous dissociated ion-pair formation, in both the absence and presence of coordinated ethylene. Full details of these results are presented in the Supporting Information.
(57) The energies listed in Figures 13 and 14 refer to ΔE_{ZPE} energies in which entropy (ΔS) and enthalpy (ΔH) corrections are not included. A relatively unfavorable entropy component for uptake of free ethylene is, however, expected to be partially compensated for by the liberation of a Me−MAO fragment similar to arguments by Lanza et al.[16]
(58) Berthomieu, D.; Bscquet, Y.; Pedocchi, L.; Goursot, A. *J. Phys. Chem. A* **1998**, *102*, 7821.
(59) Almenningen, A.; Halvorsen, S.; Haland, A. *Acta Chem. Scand.* **1971**, *25*, 1937.
(60) Huffmann, J. C.; Streib, W. E. *J. Chem. Soc. D* **1971**, 911.
(61) McGrady, G. S.; Turner, J. F. C.; Ibberson, R. M.; Prager, M. *Organometallics* **2000**, *19*, 4398.

Table 2. Calculated (DMol³/PW91/DNP) Zero-Point Energies (Δ*E*), Gibbs Free Energies (Δ*G*), Enthalpies (Δ*E*), and Entropies (*T*Δ*S*) in kcal/mol for 1/2(TMA)$_2$ + (AlOMe)$_n$

N	Al−O	Δ*E*	Δ*G*	Δ*H*	*T*Δ*S*
Present Work					
6	*ss* (**7**)	−15.7	−7.8	−15.6	−7.8
9	*sh* (**8**)	−13.0	*−7.8*[a]	*−10.1*	*−2.3*
9	*ss* (**9**)	−7.1	*−0.5*	*−5.0*	*−4.6*
Previous Work[b]					
6	*ss* (**7**)	−13.1	∼−3.0		
9	*sh* (**8**)	−9.8	∼3.5		
9	*ss* (**9**)	−4.3			

[a] The vibrational analyses for (AlOMe)$_9$ species showed spurious imaginary vibrational modes due to Me rotations that could not successfully be eliminated despite several efforts. Therefore, the calculated *T*Δ*S*, and consequently Δ*G* energies, for the (AlOMe)$_9$ species should be regarded only as estimates at the current level of theory. The thermodynamic quantities affected are indicated by italics. [b] Ref 25.

most accurate DFT results thus far reported, and good agreement is also obtained with reported MP2 results. This validates the DFT approach employed in the current study, similar to the validation strategy that was followed by Tosell.[48]

Two "classic" MAO structures, viz., (AlOMe)$_6$ (**2**) and (AlOMe)$_9$ (**3**), were selected as representative cage structures for the theoretical investigation of the conversion of "classic" MAO to TMA-expanded MAO upon interaction with TMA dimer at the current DMol³/PW91/DNP level of theory. Cleavage of a square−square (*ss*) Al−O bond in (AlOMe)$_6$ (**2**) by incorporation of one TMA unit to yield (AlOMe)$_6$−TMA (**7**) is found to proceed with Δ*E* = −15.7 kcal/mol (Table 2), in fair agreement with the ADF/BP86 Δ*E* value of −13.1 kcal/mol reported by Zurek and Ziegler.[25] For (AlOMe)$_9$ cleavage of both a square−hexagonal (*sh*) (Δ*E* = −13.0 kcal/mol), to yield **8**, and a square−square (*ss*) (Δ*E* = −7.1 kcal/mol), to yield **9**, Al−O bond is considered, as illustrated in Figure 3.

From the zero-point reaction energies (Δ*E*) summarized in Table 2 it follows that cleavage of an *sh* Al−O bond in **3** is favored to *ss* Al−O bond cleavage by 5.9 kcal/mol (ΔΔ*E*), in favorable agreement with a ΔΔ*E* of 5.5 kcal/mol that was calculated by Zurek and Ziegler.[25] In their study it was found that for all (AlOMe)$_n$ cages considered the (AlOMe)$_9$ cage is the only cage in which an *ss* Al−O bond is not calculated to be the most acidic. The higher acidity of the *sh* Al−O bond in (AlOMe)$_9$ (**3**) is indirectly related to the relatively higher steric congestion in **9** compared to **8**.

TMA versus MAO as Methylating Agents. The methylation of catalyst precursors, e.g., Cp_2ZrCl_2, prior to ethylene oligomerization catalysis is widely accepted[49−51] to be an important first stage for catalyst activation when MAO is used as cocatalyst. Understanding the nature of the methylating agent is important in order to assess its role(s) prior and during catalysis. In order to determine the possibility of MAO acting as a methylating agent, the methylation aptitudes of various MAO derivatives, including "classic" (AlOMe)$_6$ (**2**) and (AlOMe)$_9$ (**3**) and TMA-expanded MAO derivatives **7**−**9** (Figure 4), were compared to the methylating aptitude of the TMA dimer (**6**). The Me group in the methylating agent considered for methylation was determined by careful comparison of relative isomer energies for single Cl-substituted TMA and MAO structures. Figure 4 illustrates these six methylating agents together with the most likely Me group to be employed for methylation (noted by an asterisk in each case).

The methylation aptitudes were correlated to the calculated reaction energies for sequential methylation of $LCrCl_3$ (L = **10** or **11** in Figure 5) as model chromium complex according to the following general sequence:

$$LCrCl_3 \rightarrow LCrCl_2Me \rightarrow LCrClMe_2 \rightarrow LCrMe_3 \quad (2)$$

For the purpose of this study, the term "stripped-down" ligand refers to $Me_2PN(Me)PMe_2$ (**10**; also referred to as PNP−Me), while the term "full" ligand signifies $Ph_2PN(^iPr)PPh_2$ (**11**; also referred to as PNP−Ph) (Figure 5). Whereas **10** is to be considered a model of **11**, ligand **11** was recently demonstrated to yield, in combination with Cr(acac)$_3$ and MAO, a highly active ethylene trimerization/tetramerization catalyst.[6] The most appropriate bidentate PNP−Cr intermediates present during methylation were determined to be neutral Cr(III) complexes exhibiting quartet ground spin states.[52]

The sequential methylation energies of $CrCl_3$ complexes containing the two ligands **10** and **11** with each of the six methylating agents illustrated in Figure 4 are summarized in Table 3. For each methylation step both the zero-point energy (ΔE_{ZPE}) and Gibbs free energy ($\Delta G_{298.15}$) are listed for direct comparison. In addition, the total reaction energy for direct methylation of $CrCl_3$ to $CrMe_3$ is also included as the sum of the individual methylation reaction energies.

The energies calculated for the first methylation step for both "stripped-down" PNP−Me (**10**) and "full" PNP−Ph (**11**) ligand systems are found to be significantly exergonic with *TMA dimer* (**6**) *as methylating agent*. In contrast, the second and third methylation steps are calculated to be endothermic to such an extent that for PNP−Me (**10**) ΔE_{ZPE} equals 6.9 kcal/mol for the complete methylation sequence. The comparative Gibbs free energy change ($\Delta G_{298.15}$) for complete methylation of (PNP−Me)$CrCl_3$ with the TMA dimer (**6**) is lowered to 1.5 kcal/mol, albeit still endergonic. In contrast with this, it is found that expansion of the model to the more realistic (PNP−Ph)$CrCl_3$ complex yields an exergonic reaction ($\Delta G_{298.15}$ = −4.9 kcal/mol) for complete methylation ($CrCl_3 \rightarrow CrMe_3$) with TMA dimer (**6**). From these results it may thus be concluded that although the second and third methylation steps are slightly endergonic ($\Delta G_{298.15}$ = 1.0 and 2.0 kcal/mol, respectively), complete methylation is expected when excess TMA dimer is used as methylating agent.

For both the "classic" (**2** and **3**) and TMA-expanded (**7**−**9**) *MAO models* the methylation energies for all methylation steps are found to be significantly unfavorable compared to TMA dimer as methylating agent (Table 3). The increasing endergonic pattern for the second and third methylation steps is also retained for the MAO methylating agents. These results suggest that the methylating activity during catalyst activation should necessarily be due to TMA rather than MAO.

Chromacycloheptanes in the Absence of MAO. The selective oligomerization of ethylene to exclusively yield 1-hexene (trimerization) or mixtures of 1-hexene and 1-octene (tetramerization) is generally agreed to involve metallacycle intermediates.[8,11,12] This was elegantly demonstrated by the selective formation of 1-hexene after exposure of isolated chromacycloheptane complexes to ethylene.[8] In recent deuterium labeling studies Bercaw et al.[10] confirmed the importance of chromacycloheptane intermediates during PNP−Ph^{OMe}Cr(III)-catalyzed [PNP−Ph^{OMe} = (*o*-MeO−C_6H_4)$_2$PN(Me)P(*o*-MeO−C_6H_4)$_2$] ethylene trimerization. Overett et al.[11] showed from similar deuterium labeling studies that chromacycloheptane intermediates are also operating during (PNP−Ph)Cr-catalyzed ethylene trimerization, while metallacycle growth to yield chromacyclononane intermediates accounts for the tetramerization of ethylene to 1-octene. In addition, all theoretical papers

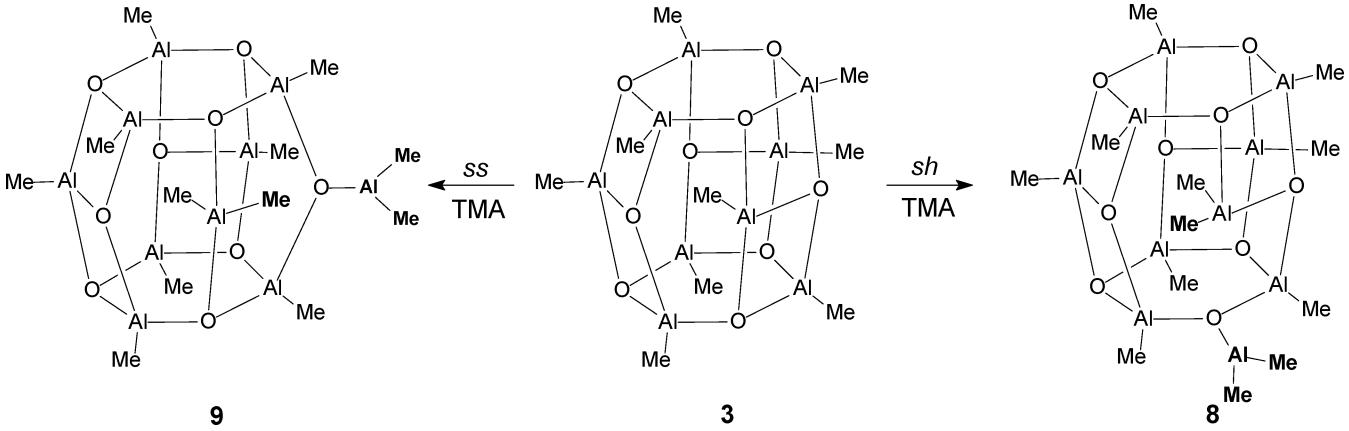

Figure 3. Interaction of TMA with both square−square (*ss*) and square−hexagonal (*sh*) Al−O bonds in "classic" $(AlOMe)_9$ (**3**).

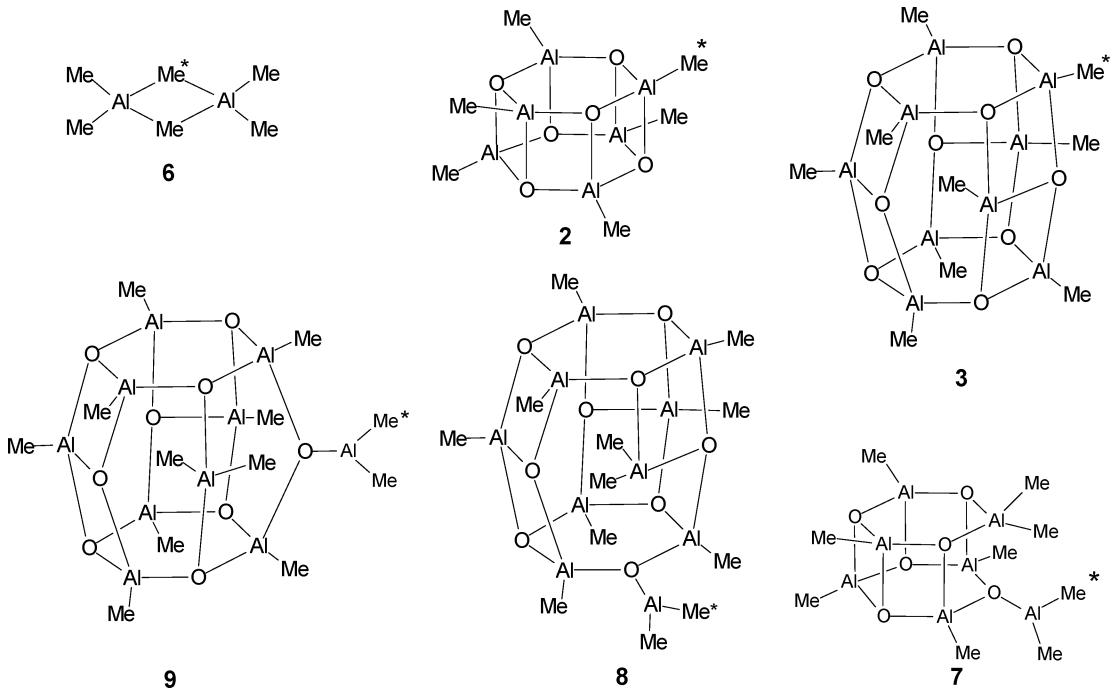

Figure 4. TMA and MAO methylating agents considered for comparison of relative methylating aptitude. (The asterisk indicates the most likely Me group utilized during methylation.)

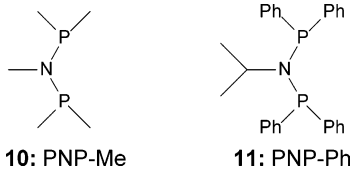

Figure 5. Structures for the "stripped-down" $Me_2PN(Me)PMe_2$ (**10**) and "full" $Ph_2PN(^iPr)PPh_2$ (**11**) ligands used in the current study.

on ethylene trimerization[12−14] consider metallacycle intermediates to rationalize the mechanism. Consequently, PNP−chromacycloheptane complexes were chosen in the current study as representative intermediates present during ethylene trimerization/tetramerization to investigate the possible interaction of MAO with an active chromium catalyst. The interaction of MAO with chromacycloheptanes, in both the absence and presence of coordinated ethylene, is considered. Two chromacycloheptane models were used, i.e., containing either "stripped-down" PNP−Me (**10** in Figure 5) or PNP−Ph (**11** in Figure 5).

Complexes of chromium are known to contain unpaired electrons in the valence shell. This is evident from recently reported magnetic susceptibility studies in which it was shown that Cr(III) complexes favor quartet spin states,[45] effectively making NMR analysis impractical. Consequently, it is important to explicitly account for the most favored Cr spin states in a computational study.[12] Formal Cr(III) oxidation states (s^1d^2) are present in the chromacycloheptane species considered in the current study, effectively making both doublet (S_1) and quartet (S_3) spin states for Cr possible. A validation study was performed in which a series of GGA exchange−correlation DFT functionals were compared for accuracy in determining different spin state energies.[52] From these comparative calculations it was found that the pure DFT functionals tend to overestimate the stability of low spin forms, in agreement with results reported by Harvey.[53] Nevertheless, it was established that the RPBE exchange−correlation functional provides results of adequate accuracy for spin state evaluations in the current application.[52] For all RPBE calculations performed on Cr(III) structures it is shown that doublet (S_1) spin state structures are significantly higher in energy than the comparative quartet (S_3) structures,[52] despite the anticipated overestimation of the doublet (S_1) stabilities.[53] Therefore, the results discussed in the remainder

Table 3. Sequential and Total Calculated Zero-Point (ΔE_{ZPE}) and Gibbs Free ($\Delta G_{298.15}$) Energies for Methylation of Stripped-Down (PNP−Me)$CrCl_3$ and Full (PNP−Ph)$CrCl_3$ Complexes with TMA Dimer (6) and MAO Derivatives 2, 3, 7−9

		(PNP−Me)$CrCl_3$		(PNP−Ph)$CrCl_3$	
agent	methylation step	ΔE_{ZPE} (kcal/mol)	$\Delta G_{298.15}$ (kcal/mol)	ΔE_{ZPE} (kcal/mol)	$\Delta G_{298.15}$ (kcal/mol)
6	first	−5.6	−7.1	−8.1	−7.9
	second	4.1	1.4	2.9	1.0
	third	8.5	7.2	4.1	2.0
	total	6.9	1.5	−1.1	−4.9
2	first	2.9	3.0	0.4	2.2
	second	12.6	11.5	11.4	11.1
	third	17.0	17.3	12.6	12.1
	total	32.4	31.8	24.5	25.4
3	first	1.5	*0.1*[a]	−0.9	*−0.7*[a]
	second	11.2	*8.6*	10.1	*8.2*
	third	15.7	*14.5*	11.3	*9.2*
	total	28.4	*23.1*	20.5	*16.8*
7	first	0.6	1.7	−1.9	0.9
	second	10.3	10.2	9.1	9.8
	third	14.7	16.1	10.3	10.8
	total	25.5	28.0	17.5	21.6
8	first	0.6	*1.8*[a]	−1.8	*1.1*[a]
	second	10.3	*10.3*	9.2	*10.0*
	third	14.7	*16.2*	10.4	*11.0*
	total	25.7	*28.4*	17.7	*22.0*
9	first	1.2	*2.4*[a]	−1.3	*1.6*[a]
	second	9.7	*10.9*	9.7	*10.5*
	third	15.3	*16.7*	10.9	*11.5*
	total	26.2	*30.0*	19.4	*23.6*

[a] The vibrational analyses for $(AlOMe)_9$ species showed spurious imaginary vibrational modes due to Me rotations that could not successfully be eliminated despite several efforts. Therefore, the thermodynamic quantities for the $(AlOMe)_9$ species should be regarded only as estimates at the current level of theory. The thermodynamic quantities affected are indicated by italics.

of this paper focus only on the quartet (S_3) Cr(III) complexes as obtained with the RPBE functional.

The current section is devoted to the nature of chromacycloheptane complexes in the *absence* of MAO. This information is required for direct comparison with complexes explicitly containing different MAO models (vide infra). Both "unsaturated" chromacycloheptanes, i.e., structures containing no coordinated ethylene, and "saturated" chromacycloheptanes, i.e., structures containing a π-coordinated ethylene in the chromium coordination sphere, are considered in this comparison. The relevance of these models for possible correlation to ethylene trimerization/tetramerization selectivities is motivated by (i) the necessary coordination of free ethylene to chromacycloheptane intermediates for eventual metallacycle growth and (ii) the need to investigate possible competition between ethylene and MAO fragments for coordination to chromium.

In Figure 6 the optimized geometries for *cationic* "stripped-down" (i.e., structures containing ligand **10**) chromacycloheptanes are illustrated in both the absence and presence of coordinated ethylene. For the "unsaturated" chromacycloheptane **12**, i.e., in the absence of coordinated ethylene, optimization yields a distorted square-pyramidal geometry in which one of the metallacycle α-carbons occupies the apical position. A prominent β-H agostic interaction (1.947 Å) occupies one of the equatorial positions. No other isomeric geometries for **12** were successfully optimized; all alternative optimizations resulted in spontaneous optimization toward **12**.

The coordination of ethylene to the cationic quartet (S_3) chromacycloheptane **12** yields the distorted octahedral geometry **13** and the distorted square-pyramidal geometry **14**. In **13** ethylene is coordinated *trans* to a β-H agostic interaction, effectively positioning the two α-carbons of the metallacycle roughly parallel to the P−Cr−P plane. The formation of **14**, in contrast, follows directly from the exchange of the β-H agostic interaction in **12** with coordinated ethylene to yield an equatorially coordinated ethylene structure containing no Cr−H agostic interactions. Weaker ethylene coordination in **14** compared to **13** is suggested by the relatively elongated Cr−ethylene distance found for **14**.

The interaction of MAO to chromium intermediates most likely involves a bridging methyl group that is shared by the chromium and the appropriate MAO cage.[19] It is therefore instructive to compare the relative energies of *neutral* chromacycloheptane complexes, in which a Me group is formally coordinated to chromium, in the absence of MAO. Figure 7 illustrates the optimized geometries for such neutral "stripped-down" (i.e., structures containing ligand **10**) chromacycloheptanes. In contrast to the single "unsaturated" cationic chromacycloheptane **12** illustrated in Figure 6, two "unsaturated" neutral complexes were successfully optimized, i.e., **15** and **16**. The geometry of **15** closely resembles **12** (Figure 6), in which a Me group is introduced to the open coordination site on Cr to yield a distorted octahedral complex with the β-H agostic interaction *cis* to the Me group. A distorted octahedral complex is also obtained for **16**, in which the β-H agostic interaction is *trans* to the Me group.

It is significant to note that **16** is calculated to be more stable than **15**. This is in contrast to results obtained for the "unsaturated" cationic chromacycles in Figure 6, where the corresponding cationic structure for **16** could not successfully be optimized; all attempts to locate the cationic equivalent of **16** resulted in the spontaneous optimization to **12** (Figure 6). It should be noted that all attempts to optimize neutral geometries in which ethylene is introduced into the chromium coordination sphere resulted in the spontaneous dissociation of ethylene.

In order to expand the "stripped-down" models illustrated in Figures 6 and 7, similar optimizations were performed with the "full" PNP−Ph ligand (ligand **11** in Figure 5). Figure 8 illustrates the optimized cationic geometries and relative energies (ΔE_{ZPE}) for both "unsaturated" and "saturated" chromacycloheptane intermediates for the PNP−Ph ligand. This data should be compared directly with the results summarized for the "stripped-down" ligand in Figure 6. Two "unsaturated" chromacycles were successfully optimized, viz., **17** and **18**. Whereas **17** corresponds to **12** (Figure 6), the "stripped-down" equivalent corresponding to **18** could not successfully be optimized (vide supra). The relative energies for these "unsaturated" chromacycloheptanes favor **17** over **18** by $\Delta E_{ZPE} = 2.0$ kcal/mol.

Similar ethylene coordination modes were located for the "full" complexes, as was found for the "stripped-down" complexes (Figure 6) and is illustrated as **19** and **20** in Figure 8. Ethylene coordination *trans* to the β-H agostic interaction in **19** is favored over equatorial β-H displacement (**20**) by 1.3 kcal/mol, which mirrors the results obtained for the "stripped-down" structures (Figure 6).

Neutral chromacycloheptane structures, containing a formally coordinated methyl group, were also successfully optimized for the "full" PNP−Ph ligand as illustrated in Figure 9. The two complexes **21** and **22** are geometrically similar to the respective "stripped-down" complexes **15** and **16** (Figure 7). However, the change introduced by the more realistic ligand is reflected in the relative energies, albeit that the relative trends observed for the "stripped-down" ligand structures are retained. Structure **22** is calculated to be lower in energy than **21** by $\Delta E_{ZPE} = 10.0$ kcal/mol compared to a ΔE_{ZPE} of 5.5 kcal/mol for the corre-

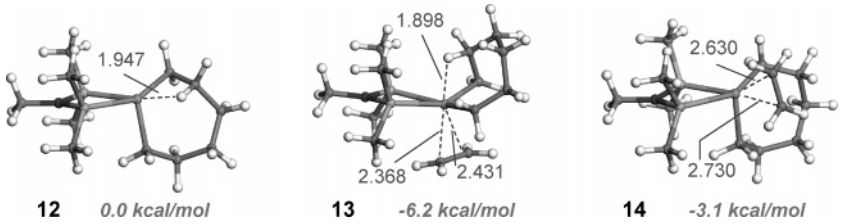

Figure 6. Optimized geometries for "stripped-down" (ligand **10**) cationic chromacycloheptane structures in both the absence and presence of coordinated ethylene. (Bond lengths in Å and ΔE_{ZPE} energies in kcal/mol relative to **12** are balanced with the energy of free ethylene where necessary.)

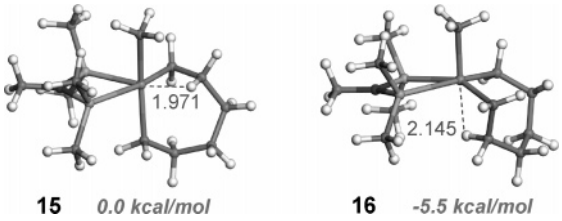

Figure 7. Optimized geometries for "stripped-down" (ligand **10**) neutral chromacycloheptane structures. (Bond lengths in Å and ΔE_{ZPE} energies in kcal/mol relative to **15**.)

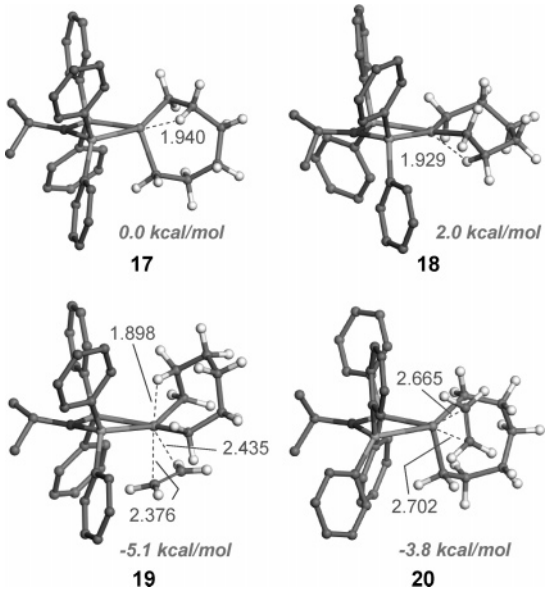

Figure 8. Optimized geometries for "full" (ligand **10**) cationic chromacycloheptane structures in both the absence and presence of coordinated ethylene. (Bond lengths in Å and ΔE_{ZPE} energies in kcal/mol relative to **17** are balanced with the energy of free ethylene where necessary; hydrogens on the ligand are omitted to ensure clarity.)

sponding "stripped-down" complexes (Figure 7). Once again, no neutral complexes were successfully located with ethylene formally incorporated into the chromium coordination sphere.

"Stripped-Down" Chromacycloheptanes in the Presence of $(AlOMe)_6$−TMA (7). The cocatalysts in, for example, metallocene-catalyzed polymerizations are widely accepted to facilitate the generation of ion-pair complexes in which a cationic transition metal complex is paired with an anionic cocatalyst fragment.[1] In this regard, a number of theoretical studies aimed at probing the fundamental role of boron-based cocatalysts, e.g., $B(C_6F_5)_3$, with metallocenes have been reported.[16,18] From these studies it is argued that the interaction of the cocatalyst with the metal occurs via a bridging methyl group. This interaction generates a catalyst/cocatalyst "dissociated" ion-pair complex after abstraction of a methyl group from an appropriate methylated catalyst precursor. A similar interaction is envisaged for "activated" MAO with a methylated catalyst precursor or intermediate. In particular, Zurek and Ziegler reported[25] a relevant theoretical study in which the explicit incorporation of a model for TMA-expanded MAO, i.e., $(AlOMe)_6$ activated by 1 TMA unit, was used. In another report by Rappé et al.[54] the $(AlOMe)_9$ cluster was considered an appropriate model for such theoretical studies.

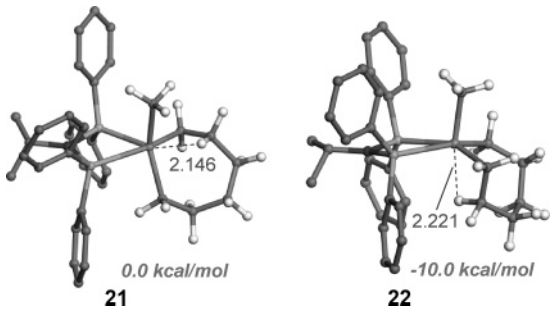

Figure 9. Optimized geometries for "full" (ligand **11**) neutral chromacycloheptane structures. (Bond lengths in Å and ΔE_{ZPE} energies in kcal/mol relative to **21**; hydrogens on the ligand are omitted to ensure clarity.)

In order to assess the similar possibility of interaction of TMA-expanded MAO with an active chromium intermediate, the coordination of $(AlOMe)_6$−TMA (**7**) to "stripped-down" (PNP−Me ligand) chromacycloheptane intermediates was investigated. The interaction of *neutral* $(AlOMe)_6$−TMA (**7**) with *neutral* chromacycloheptanes was modeled by coordination of the unsaturated three-coordinate Al atom in **7** with the methyl group of the neutral chromacycloheptanes. This interaction mode and the notation used are illustrated for a representative complex in Figure 10 (this structure corresponds to **23** in Figure 11). The use of these smaller models facilitated relatively expedient initial calculations, which were used in turn for expansion to more realistic models discussed later.

Figure 11 illustrates geometrical and relative energy (ΔE_{ZPE}) data for optimized chromacycloheptane geometries bridged by a methyl group to $(AlOMe)_6$−TMA (**7**). The metallacycle conformation in **23** contains a β-H agostic interaction roughly in the P−Cr−P plane and is similar to the metallacycle conformation depicted for **15** in Figure 7. In **24** a β-H agostic interaction is *trans* to the bridging Me group with both metallacycle α-carbons roughly in the P−Cr−P plane, similar to the metallacycle conformation illustrated for **16** in Figure 7. A third metallacycle complex (**25**), which contains no β-H agostic interactions and both metallacycle α-carbons in the P−Cr−P plane, was also located. The conformation of the chromacycle in **25** represents a boat structure similar to the expected conformation of cyclohexane. This boat conformation is retained upon coordination of ethylene in **26** to yield a distorted octahedral complex. These schematic representations for the specific chromacycle conformations are consistently used in the remainder of this paper.

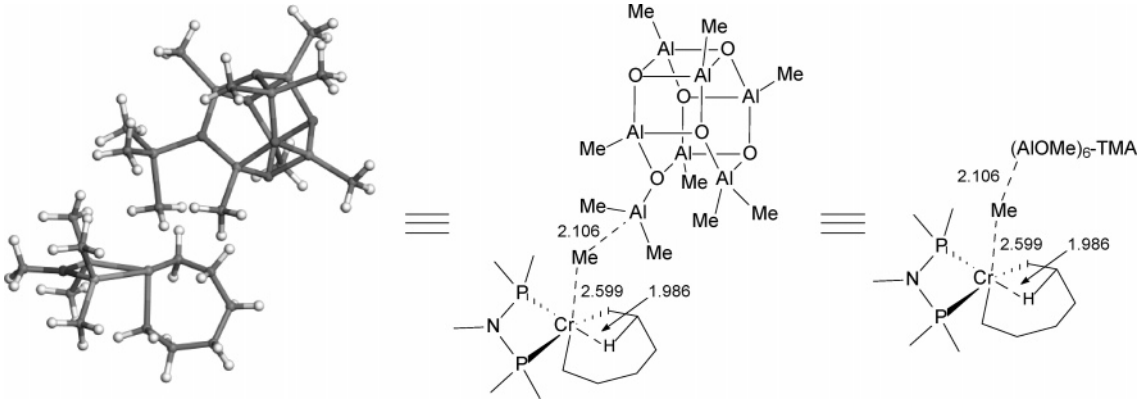

Figure 10. Example of an optimized geometry for $(AlOMe)_6$−TMA (**7**) interaction with a representative "stripped-down" (PNP−Me ligand) chromacycloheptane.

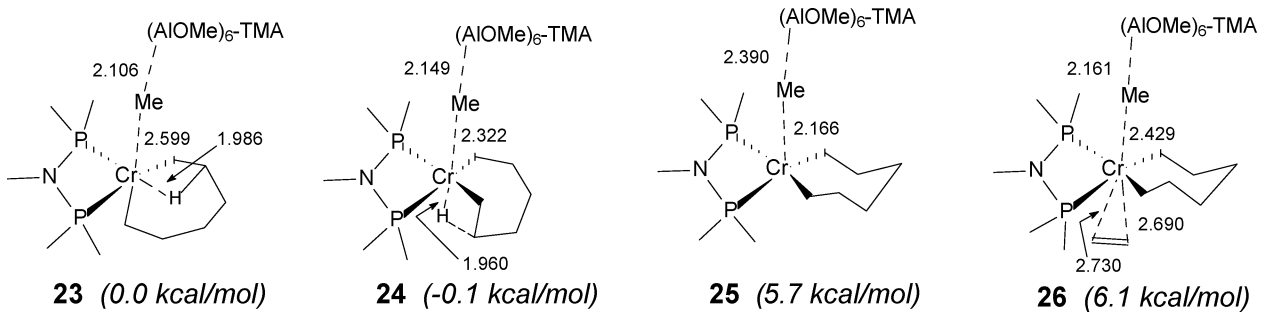

Figure 11. Optimized geometries of "stripped-down" (ligand **10**) chromacycloheptane complexes bridged via a methyl group to $(AlOMe)_6$−TMA (**7**), in both the absence and presence of coordinated ethylene. (Bond lengths in Å and ΔE_{ZPE} energies in kcal/mol relative to **23**.)

Formal coordination of the $(AlOMe)_6$−TMA (**7**) fragment in **23** is evident from the relatively short calculated Cr−Me and Me−Al distances of 2.599 and 2.106 Å, respectively. However, the interaction of the Me group with Al is evident from the elongation of the Cr−Me distance from 2.187 Å, when $(AlOMe)_6$−TMA (**7**) is not present (**15**, Figure 7), to 2.599 Å in **23**. A similar trend is found for **24**: the β-H agostic interaction *trans* to the bridging Me group is shortened from 2.145 Å in **16** (Figure 7) to 1.960 Å in **24**. This may conveniently be explained by the partial positive charge on Cr upon elongation of the Cr−Me distance from 2.098 Å in **16** (Figure 7) to 2.322 Å in **24**. The Cr−Me distance in **25** is shorter compared to **23** and **24** and is presumably caused by a relatively higher partial positive charge on Cr in **25** due to the lack of additional β-H agostic interactions. A comparison of the relative Cr−Me and Me−Al distances in **23**, **24**, and **25** clearly shows that Cr and Al compete for interaction with the bridging Me functionality, evident from the inverse dependence of Cr−Me and Me−Al distances. The relative ΔE_{ZPE} values for **23**, **24**, and **25** indicate that both **23** and **24**, containing additional β-H agostic stabilization, are favored above the coordinatively unsaturated chromacycloheptane **25**.

The successful optimization of the *ethylene-coordinated structure* **26** is significant, because a similar structure in the absence of $(AlOMe)_6$−TMA (**7**) was not successfully located (vide supra). Partial abstraction of the Me group in **26** leads to enhanced partial positive charge on Cr, *effectively facilitating the* π*-coordination of ethylene*. This is highlighted by the elongation of the Cr−Me distance in **26** compared with the precursor complex **25**. The relatively elongated ethylene−chromium distances in **26** (2.730 and 2.690 Å), as well as unfavorable ethylene coordination energy (ΔE_{ZPE} = 6.1 kcal/mol relative to **23** and free ethylene), suggest a relatively weak ethylene interaction.

"Full" Chromacycloheptanes in the Presence of $(AlOMe)_9$−TMA Models. In this section an expansion of the models, with regard to both the chromacycloheptanes and MAO models, is presented to ensure a more comprehensive and realistic account of the interaction between MAO and an active ethylene trimerization/tetramerization chromium intermediate. For this purpose the "stripped-down" PNP−Me ligand (ligand **10** in Figure 5) used in the previous section is replaced by the "full" PNP−Ph ligand (ligand **11** in Figure 5), a bidentate ligand known for its tetramerization activity in combination with chromium and MAO.[6] The "stripped-down" MAO model, $(AlOMe)_6$−TMA (**7**), is replaced with the more appropriate $(AlOMe)_9$ cage structure, activated by a single TMA unit. As indicated above in Figure 3, the TMA-induced cleavage of square−hexagonal (*sh*) and square−square (*ss*) Al−O bonds in the $(AlOMe)_9$ cage [to yield $(AlOMe)_9$−TMA-*sh* (**8**) and $(AlOMe)_9$−TMA-*ss* (**9**), respectively] leads to two TMA-expanded MAO models for incorporation in the current study. In Table 2 it was shown that the formation of **8** from $(AlOMe)_9$ is favored over the formation of **9**. However, due to the underlying uncertainty and complexity of active MAO structures during catalysis, it was decided to study the Cr−MAO interaction with both **8** and **9**, effectively covering a more comprehensive range of structures and representing a more inclusive account of actual catalyst/MAO interactions. In the discussion to follow, the DFT (RPBE) results obtained for the interaction of the neutral $(AlOMe)_9$−TMA models **8** and **9** with neutral methylated PNP−Ph-chromacycloheptanes (as summarized in Figure 9) focus on $(AlOMe)_9$−TMA interacting with (i) "unsaturated", i.e., in the absence of ethylene, chromacycloheptanes for the most relevant quartet (S_3) chromium spin states and (ii) "saturated", i.e., in the presence of coordinated ethylene, chromacycloheptanes. Figure 12 illustrates an example of the optimized geometry of one of these TMA-expanded MAO−

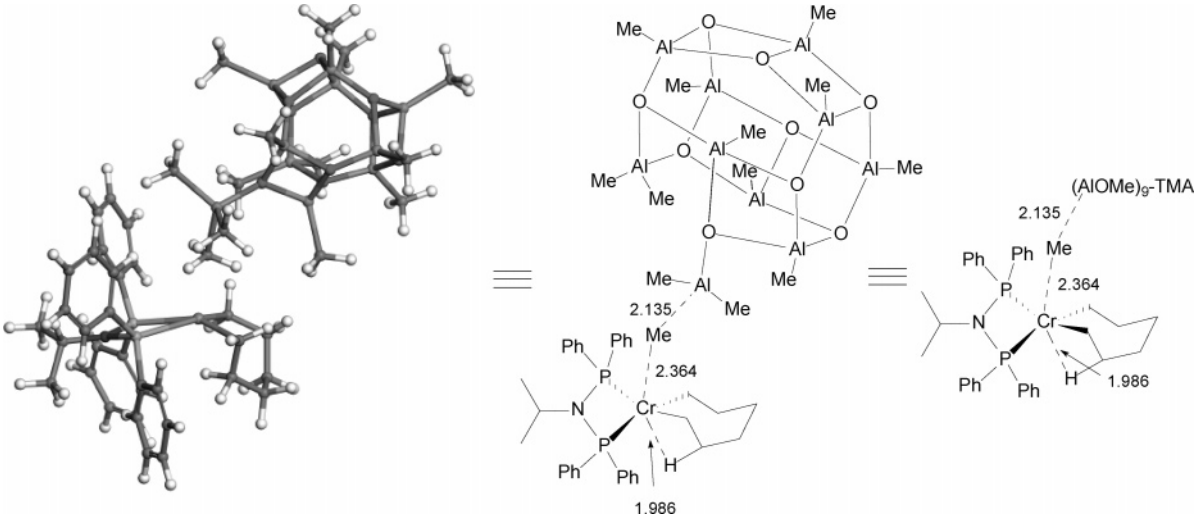

Figure 12. Example of an optimized geometry for $(AlOMe)_9$−TMA-*sh* (**8**) interaction with the "full" PNP−Ph-chromacycloheptane **22** to yield **27** (Figure 13).

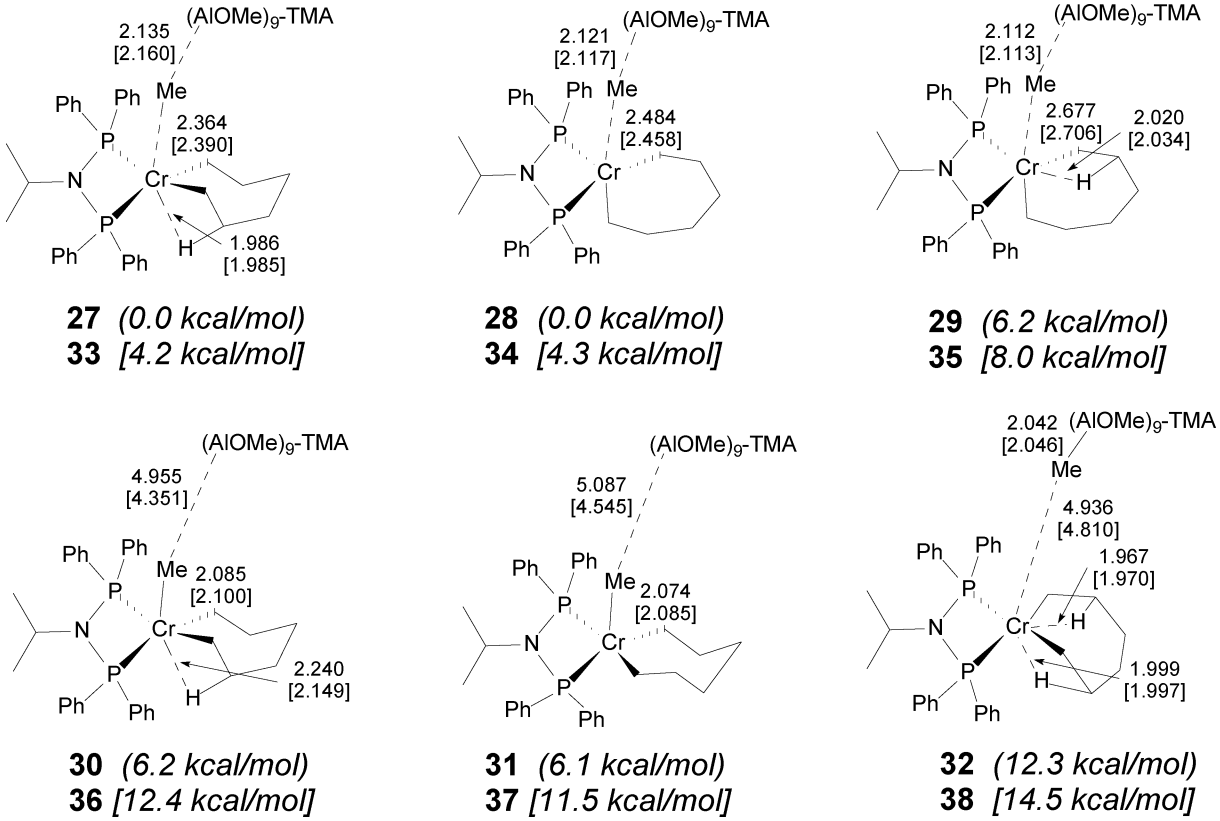

Figure 13. DMol[3]/RPBE-optimized geometries for interaction of $(AlOMe)_9$−TMA-*sh* (**8**) and $(AlOMe)_9$−TMA-*ss* (**9**) with "unsaturated" PNP−Ph chromacycloheptane complexes. Comparative ΔE_{ZPE} energies (kcal/mol) are presented relative to the lowest energy structure **27**. All data pertaining to $(AlOMe)_9$−TMA-*ss* (**9**) are denoted in square brackets to distinguish it from the data for $(AlOMe)_9$−TMA-*sh* (**8**).

chromacycloheptane structures, in which (AlOMe)−TMA-*sh* (**8**) is bridged via a methyl group to a chromacycloheptane (this structure corresponds to **27** in Figure 13).

Figure 13 illustrates the optimized geometries for interaction of both $(AlOMe)_9$−TMA-*sh* (**8**) and $(AlOMe)_9$−TMA-*ss* (**9**) to "unsaturated" methylated PNP−Ph-chromacycloheptanes, along with the relative ΔE_{ZPE} energies. In order to distinguish the geometrical and energy data for interaction of **8** and **9**, all data pertaining to $(AlOMe)_9$−TMA-*ss* (**9**) in Figure 13 are denoted by square brackets.

For all the structures illustrated in Figure 13 the interaction of $(AlOMe)_9$−TMA with the chromacycloheptane involves bridging of the three-coordinate Al in **8** and **9** with the methyl functionality on chromium (see Figure 12). In the β-H agostic structures **27** and **33**, relatively tight coordination of **8** and **9**, respectively, is evident from the relatively short Cr−Me and Me−Al distances, in good agreement with the structural parameters that were obtained for the "stripped-down" model **23** (Figure 11). The optimized structures lacking β-H agostic interactions in the metallacycle backbone (**28** and **34**) yield bridging methyls with elongated Cr−Me distances compared to **27** and **33**, respectively, despite the lower chromium coordination number in **28** and **34**. In the three-dimensional geometry of **27** (Figure 12, similar for **33**), the agostic β-H is

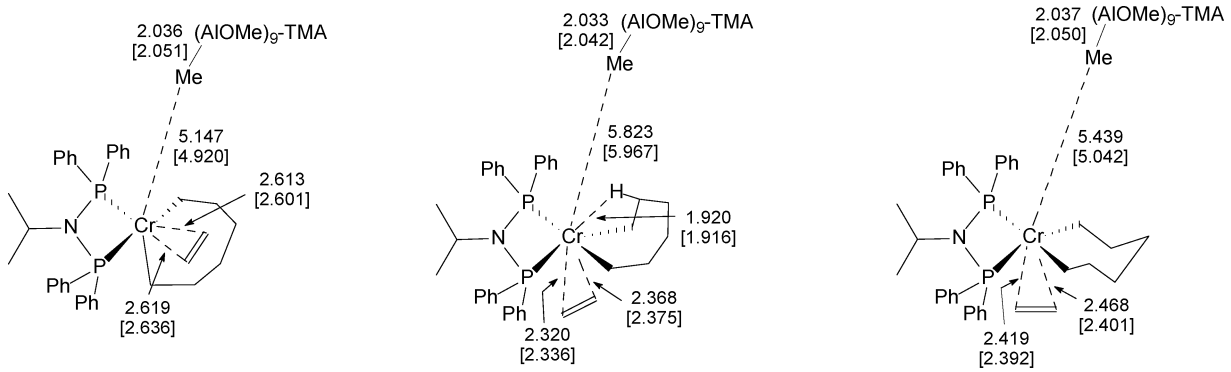

Figure 14. DMol[3]/RPBE-optimized geometries for interaction of $(AlOMe)_9$−TMA-*sh* (**8**) and $(AlOMe)_9$−TMA-*ss* (**9**) with "saturated" PNP−Ph chromacycloheptane complexes. Comparative ΔE_{ZPE} energies (kcal/mol) are presented relative to the lowest energy structure **27** (Figure 13) and free ethylene. All data pertaining to $(AlOMe)_9$−TMA-*ss* (**9**) are denoted in square brackets to distinguish it from the data for $(AlOMe)_9$−TMA-*sh* (**8**).

orientated *trans* to the bridging methyl. In contrast, a methylene fragment occupies the position *trans* to the bridging methyl in both **28** and **34**, causing a more pronounced *trans* influence, which presumably accounts for the elongated Cr−Me distances for the latter. It is interesting to note that the relative energies of **27** and **28**, and **33** and **34**, are essentially the same. Upon formation of a β-H agostic interaction *cis* to the bridging methyl group, to yield **29** and **35**, respectively, an unexpected increase in relative energy (by 3.7−6.2 kcal/mol), compared to the corresponding metallacycles lacking β-H agostic interactions (**28** and **34**), is found. The relative increase in the Cr−Me distances in **29** and **35** seems to suggest that this energy trend is due to unfavorable steric congestion upon formation of the *cis* β-H agostic interaction.

In an attempt to assess the influence of this steric congestion, structures in which neutral $(AlOMe)_9$−TMA-*sh* (**8**) and $(AlOMe)_9$−TMA-*ss* (**9**) are dissociated from the corresponding chromacycloheptanes were optimized, yielding **30**, **31**, **36**, and **37**. The neutral dissociated structures are found to be higher in energy compared to the low-energy counterparts (**27**, **28**, **33**, and **34**) by 6.1−8.2 kcal/mol, effectively suggesting that saturation of Al in the MAO fragment favorably overcomes the steric congestion experienced by a tightly coordinated $(AlOMe)_9$−TMA fragment for these chromacycloheptanes in the absence of ethylene.

Formal abstraction of the methyl group from chromium leads to the optimization of the "dissociated" ion-pairs **32** and **38**, exhibiting Cr−Me distances of ca. 5 Å. The unexpected formation of double β-H agostic interactions in the metallacycle backbones was found to be necessary for retention of the dissociated state of the anionic MAO fragment; efforts to optimize structures in which one of the β-H agostic interactions is broken or optimization initiated from a single β-H agostic precursor resulted in formal recoordination of MAO via the methyl bridge. Formation of **32** and **38** is, however, energetically unfavorable, which may be attributed to either unfavorable methyl abstraction and/or unfavorable formation of the double β-H agostic interaction in the metallacycle backbone. In addition, it should be noted that the gas-phase calculations reported here would necessarily be biased toward structures in which charge separation does not occur.

Figure 14 illustrates the optimized geometries, and relative ΔE_{ZPE} energies, for interaction of both $(AlOMe)_9$−TMA-*sh* (**8**) and $(AlOMe)_9$−TMA-*ss* (**9**) with "saturated" chromacycloheptane intermediates, i.e., in the presence of coordinated ethylene. Three chromacycloheptane−MAO structures were successfully optimized for each $(AlOMe)_9$−TMA isomer, yielding a total of six geometries. The most important observation to be made from Figure 14 is that *no structures were successfully optimized in which the bridging methyl remains formally coordinated to chromium*; that is, Cr−Me distances are >5 Å in all cases. This shows that competition between ethylene and the methyl group to coordinate to chromium occurs. This further implies that the uptake of ethylene is necessary to afford formal methyl abstraction by the MAO.

The most likely coordination mode for ethylene in the presence of **8** is in the plane defined by P−Cr−P, as illustrated for **39**. The Cr−ethylene distances in **39** of 2.613 and 2.619 Å are significantly longer than the corresponding distances for ethylene coordinated perpendicular to the P−Cr−P plane in **40** (2.368 and 2.320 Å). In **40** an additional β-H agostic interaction is present *trans* to the coordinated ethylene, which leads to an elongated Cr−Me distance of 5.823 Å and increasing its energy relative to **39** by 0.7 kcal/mol. The stabilization effect of the β-H agostic interaction in **40** is estimated from the 5.0 kcal/mol higher energy of complex **41**, in which no β-H agostic interactions are present.

Similar ethylene coordination complexes in the presence of **9** were successfully optimized. However, a reversal in the relative energies for the axially (**43**) and equatorially (**42**) coordinated ethylene complexes (compared to **39** and **40**) was found, the former calculated to be favored by 2.2 kcal/mol. The chromacycloheptane structure containing no β-H agostic interactions (**44**) is found to be significantly higher in energy than **43** by 9.1 kcal/mol. Structure **43** is calculated to be less stable than **39** by 1.6 kcal/mol, retaining the general trend of lower relative energies for the chromacycloheptane complexes containing $(AlOMe)_9$−TMA-*sh* (**8**).

Discussion

Two $(AlOMe)_n$ cage sizes with $n = 6$ and 9 were chosen as representative models for the structure of "classic" MAO (see **2** and **3** in Figure 1). The selection of $(AlOMe)_6$ is in agreement with the model used in theoretical studies on the interaction of MAO as cocatalyst in zirconocene-catalyzed olefin polymerization.[19] It was also found that the $(AlOMe)_6$ cage represents the smallest cage structure containing both hexagonal and square faces, but it is not particularly abundant compared to the larger cage structures. Consequently, in the current study the "smaller"

$(AlOMe)_6$ cage is considered a "stripped-down" version of the more "realistic" $(AlOMe)_9$ cage models. Expansion of the model from $(AlOMe)_6$ to $(AlOMe)_9$ is motivated by the predicted distribution of cage structures[25] in which it was found that the $(AlOMe)_9$ cage is among the most abundant cage structures containing strained square−square (*ss*) bonds necessary for activation by reaction with TMA. To the best of our knowledge, the incorporation of $(AlOMe)_9$ cage structures to theoretically investigate interactions with transition metal complexes is restricted to short references by Rappé et al. in a review paper.[54] It should be noted though that alternative MAO cage structures have also been used in theoretical studies, as is evident from recent reports.[20,21]

In the current study the "activation" of "classic" MAO is represented by the reaction of a single TMA unit with $(AlOMe)_6$ (**2**) and $(AlOMe)_9$ (**3**) to yield $(AlOMe)_6$−TMA (**7**), $(AlOMe)_9$−TMA-*sh* (**8**), and $(AlOMe)_9$−TMA-*ss* (**9**) in Figure 4. Whereas the formation of **7** is calculated to proceed from **2** and free TMA dimer by cleavage of a *square*−*square* Al−O bond with a ΔE_{ZPE} of −15.7 kcal/mol, the cleavage of a *square*−*hexagonal* Al−O bond in **3** is found to proceed with a ΔE_{ZPE} favored by 5.9 kcal/mol compared to cleavage of the corresponding *square*−*square* Al−O bond (Table 2), in agreement with other published results.[25] Notwithstanding the anticipated higher latent Lewis acidity of the *square*−*square* Al−O bond in **3**, the resulting higher steric congestion of the product **9** compared to the *square*−*hexagonal* Al−O cleaved product **8** results in the latter being designated as the best representative TMA-expanded MAO model for the current study.

Elucidation of the exact mechanism for metallocene activation for polymerization in the presence of MAO is plagued by the elusive structure of active MAO.[1] In this context it is thus difficult to assess whether MAO itself or the TMA present in MAO is responsible for catalyst activation. Although it is widely accepted that the activation process of metallocene catalysts involves methylation followed by abstraction of a methyl group,[1] the independent catalyst/cocatalyst interactions of TMA and MAO are not conclusive. For instance, it is well known that Cp_2ZrCl_2 rapidly reacts with MAO to yield the monomethylated complex $Cp_2Zr(Me)Cl$ and that the addition of excess MAO leads to the fully methylated complex Cp_2ZrMe_2.[49] It is argued that the first methylation step is afforded either by TMA contained in MAO or by MAO itself, whereas the second methylation step occurs via Cl abstraction by MAO.[50]

In order to determine the importance of MAO for the activation of Cr catalyst precursors, the reaction energies for the sequential methylation of the quartet $(PNP)CrCl_3$ catalyst precursor (PNP represents the bidentate phosphine ligands **10** and **11** illustrated in Figure 5) were calculated (Table 1). The methylating aptitude of the TMA dimer was compared to the methylating aptitudes of "classic" and TMA-expanded MAO cage models, as illustrated in Figure 4. From the relative reaction energies it was found that the methylating aptitude of TMA dimer is superior to all the MAO models considered. In all cases the *first* methylation step exhibited the most favorable reaction energies. However, whereas it was found to be significantly exothermic for TMA dimer, most of the MAO models exhibited only a slight exothermic first methylation step. The *second* and *third* methylation steps were endothermic for all the methylating agents considered. In contrast to the MAO models, the overall energy of methylation by TMA dimer, i.e., $CrCl_3 \rightarrow CrMe_3$, was calculated to be exothermic for the most realistic Cr complex (containing ligand **11** in Figure 5). These theoretical results support the notion that free TMA, either present in the composition of MAO or added, is responsible for the methylation of Cr precursors during initiation, effectively eliminating competing methylation by MAO in the presence of free TMA. Additionally, the complete methylation to $(PNP)CrMe_3$ complexes is expected in the presence of excess TMA. Note that this conclusion should be differentiated from the relative aptitudes of TMA and MAO to afford "dissociated" ion-pair complexes, i.e., by formally abstracting a methyl group.

The selective ethylene oligomerization afforded by PNP-based Cr complexes to yield 1-hexene and 1-octene in high yields[6,7,55] was established from deuterium-labeling studies to involve Cr metallacycle intermediates.[11] It was therefore deemed appropriate to use a chromacycloheptane structure as model Cr complex to study possible interactions with MAO models. From both the calculated[52] results and experimental evidence[45] it is established that the ground state of the Cr(III) metallacycle structures is a quartet (S_3). The use of "stripped-down" Cr−MAO models (i.e., the PNP−Me ligand (**10**; Figure 5) and $(AlOMe)_6$−TMA (**7**; Figure 4) as MAO model] does not provide similar results to those obtained for the "full" Cr−MAO models (i.e., the PNP−Ph ligand (**11**; Figure 5) and $(AlOMe)_9$−TMA (**8** and **9**; Figure 4) as MAO models] when MAO interaction via a methyl bridge with Cr is optimized. This is particularly evident from the tight coordination of MAO to chromium upon coordination of ethylene in the "stripped-down" complex **26** (Figure 11), compared to spontaneous methyl abstraction from chromium upon introduction of ethylene in all the "full" complexes illustrated in Figure 14. This highlights the importance of choosing an appropriate MAO model.[56]

For all the "full" Cr−MAO complexes illustrated in Figure 13 it follows that tight coordination of MAO via a methyl bridge to the chromacycloheptane complexes prevails as the lowest energy structures in the *absence of ethylene*. This is evident from the relatively short Cr−Me and Me−Al distances of 2.364 and 2.135 Å and 2.390 and 2.160 Å for **27** and **33** (Figure 13), respectively. However, formal abstraction of the methyl group from chromium (in the *absence* of ethylene), to yield **32** and **38** (Figure 13), is calculated to proceed with surprisingly low endothermicities of 12.3 and 10.3 kcal/mol compared to **27** and **33**, respectively. This result is significant when it is taken into consideration that the current DFT calculations are performed in the gas phase, effectively representing a perfect nonpolar medium. Although trimerization/tetramerization catalysis is mostly performed in nonpolar solvents, it is envisaged that the theoretical approach followed here will tend to overestimate effects due to the nonpolar medium, such as the energy required for formal charge separation during methyl group abstraction from chromium. In a similar sense it may thus be argued that if abstraction of the bridging methyl group is found to proceed with relatively low energies in the current gas-phase DFT analysis, methyl group abstraction in actual experiments is likely to be even more favorable where a solvent is formally introduced. Indeed, from the gas-phase calculations it is found that introduction of ethylene results in the spontaneous elongation of Cr−Me distances, which represents the lowest energy structures when ethylene is incorporated in the models (Figure 14). It is therefore conceivable that the formation of these "dissociated" ion-pair structures (Figure 14), exhibiting Cr−Me distances of ∼5 Å, are likely during actual catalysis, especially for ethylene coordination processes. This is supported by the relatively low endothermic reaction energies of 6.6 and 4.0 kcal/mol calculated for **27** + ethylene → **39** and **33** + ethylene → **43**, respectively (Figures 13 and 14).[57]

Table 4. Total Calculated Hirshfeld Charges (q^H) Located on the Me−MAO Fragments of Selected Optimized Geometries

figure	structure	q^H Me--MAO	Cr--Me (Å)
No MAO			
6	**16**	−0.250	2.098
8	**22**	−0.235	2.077
$(AlOMe)_6$−TMA			
10	**24**	−0.579	2.322
$(AlOMe)_9$−TMA-sh			
12	**27**	−0.574	2.364
12	**28**	−0.666	2.484
12	**29**	−0.729	2.677
12	**32**	−0.910	4.936
13	**39**	−0.826	5.147
13	**40**	−0.839	5.823
$(AlOMe)_9$−TMA-ss			
12	**33**	−0.618	2.390
12	**34**	−0.660	2.458
12	**35**	−0.725	2.706
12	**38**	−0.894	4.810
13	**42**	−0.827	4.920
13	**43**	−0.794	5.967
TMA			
15	**44**	−0.463	2.130
15	**45**	−0.592	4.327
15	**46**	−0.557	5.015
15	**47**	−0.562	5.967

An investigation of charge delocalization prior and after the formation of "dissociated" ion-pair chromacycloheptane−MAO structures was carried out by calculation of the total Hirshfeld charge (q^H)[44] located on the Me−MAO fragment of selected structures (Table 4). In the absence of MAO, the relative charge (q^H) located on the methyl group designated for abstraction is −0.250 and −0.235 for the "stripped-down" (**16**; Figure 7) and "full" (**22**; Figure 9) chromacycloheptanes, respectively. This shows that a significant fraction negative charge is already located on the methyl groups of the neutral complex prior to interaction with MAO.

Interaction of the "stripped-down" MAO model $(AlOMe)_6$−TMA (**7**) with **16** leads to the tightly coordinated Cr−MAO complex **24**, which is bridged by the methyl group. The charge (q^H) located on the Me−MAO fragment of **24** is calculated to be −0.579, which indicates that a significant distribution of negative charge from the free Me−chromacycloheptane fragment **16** to MAO occurs upon coordination of MAO. A similar negative charge delocalization to −0.574 and −0.618 is found for coordination of the "full" MAO models, $(AlOMe)_9$−TMA-*sh* (**8**) and $(AlOMe)_9$−TMA-*ss* (**9**), to the more realistic chromacycloheptane complex **22** to yield **27** and **33**, respectively. From the data summarized for the $(AlOMe)_9$−TMA-*sh* (**8**)/**22** interaction in Table 4, it is evident that a direct correlation exists between the amount of negative charge located on the Me−MAO fragment and the corresponding Cr−Me distances: for the tightly coordinated complex **27** (Cr−Me: 2.364 Å) q^H equals −0.574, whereas for the "dissociated" ion-pair **32** (Cr−Me: 4.936 Å) q^H equals −0.910, resembling almost complete charge separation. Coordination of ethylene leads to slightly less negative charge distribution to the Me−MAO fragments in **39** and **40**, suggesting marginally weaker electrostatic interactions between MAO and chromium. Similar trends are found for the $(AlOMe)_9$−TMA-*ss* (**9**)/**22** interaction.

In order to assess the significance of the charge separations and relative energies calculated for the MAO models, four geometries were optimized in which TMA interacts with chromium similar to the Cr−MAO interactions. Geometrical parameters and relative energies for these Cr−TMA complexes are summarized in Figure 15 and may be compared directly to the corresponding structures for Cr−MAO in Figures 13 and 14.

Dissociation of the tightly coordinated TMA fragment in **44** requires 22.1 kcal/mol to yield the "dissociated" ion-pair **45**. This should be contrasted to calculated energy requirements of only 12.3 and 10.2 kcal/mol for similar transformations involving $(AlOMe)_9$−TMA-*sh* (**8**; **27** → **32**) and $(AlOMe)_9$−TMA-*ss* (**9**; **33** → **38**) in Figure 13. The total negative charge on the Me−TMA fragment in **44** changes from −0.463 to −0.592 upon formation of the "dissociated" ion-pair **45** (Table 4). This amounts to an increase in negative charge of only 0.129, which is in contrast to an increase of 0.336 negative charge for "dissociated" ion-pair formation from the corresponding MAO complex (**27** → **32**; Table 4). Coordination of ethylene to **44** results in the formation of **46** and **47** with an increase in energy of 21.8 and 13.0 kcal/mol, respectively. Significantly lower energy changes are found for similar transformations with MAO; for example, the corresponding MAO structures **41** and **40** (Figure 14) are formed with respective energies of 12.3 and 7.3 kcal/mol relative to the precursor **27** and free ethylene. Once again, the total negative charges on the Me−TMA fragments of the "dissociated" ion-pairs (**46** and **47**, Table 4) are significantly lower than the charge distribution on corresponding Cr−MAO complexes (e.g., **41** and **40**, Table 4). From these comparative results for TMA and MAO it is thus evident that the abstraction of a methyl group from Cr by TMA requires significantly more energy than corresponding methyl abstraction by MAO. Furthermore, this phenomenon may be correlated to the relative capacities of TMA and MAO to accommodate a negative charge upon formation of the "dissociated" ion-pair complexes. From the Hirshfeld charge analyses it follows that the negative charge is more smoothly accommodated by MAO.

The hypothesis[33] that "free" TMA, and not MAO, could act as cocatalyst in a metallocene−MAO-based system is thus not supported by the "activated" MAO and "free" TMA theoretical results presented here for the chromacycloheptane models. In addition, unlike the activation of Cp_2ZrMe_2 with MAO, the equilibrium for TMA interaction with Cp_2ZrMe_2 lies far to the left.[38]

$$Cp_2ZrMe_2 + Me_3Al \rightleftharpoons Cp_2ZrMe^+AlMe_4^- \qquad (3)$$

From these experimental results and the theoretical results presented here it may thus be concluded that MAO is a significantly stronger Lewis acid than TMA, effectively resulting in a counterion that is less coordinating than a counterion derived from TMA. It is thus unlikely that "free" TMA will compete with MAO in facilitating the essential formation of "dissociated" ion-pair complexes.

Conclusions

In this study a DFT investigation on the interaction of MAO models with chromacycloheptane complexes is presented. Chromacycloheptane intermediates are known to be important catalytic intermediates during the selective trimerization and tetramerization of ethylene to 1-hexene and 1-octene, respectively. In particular, chromacycloheptane models containing bidentate "stripped-down" $Me_2PN(Me)PMe_2$ and "full" $Ph_2PN(^iPr)PPh_2$ ligands were optimized in both the absence and presence of MAO models to gain insight into the possible roles played by MAO during selective ethylene oligomerization catalysis. Two "classic" MAO cage structures, $(AlOMe)_6$ and

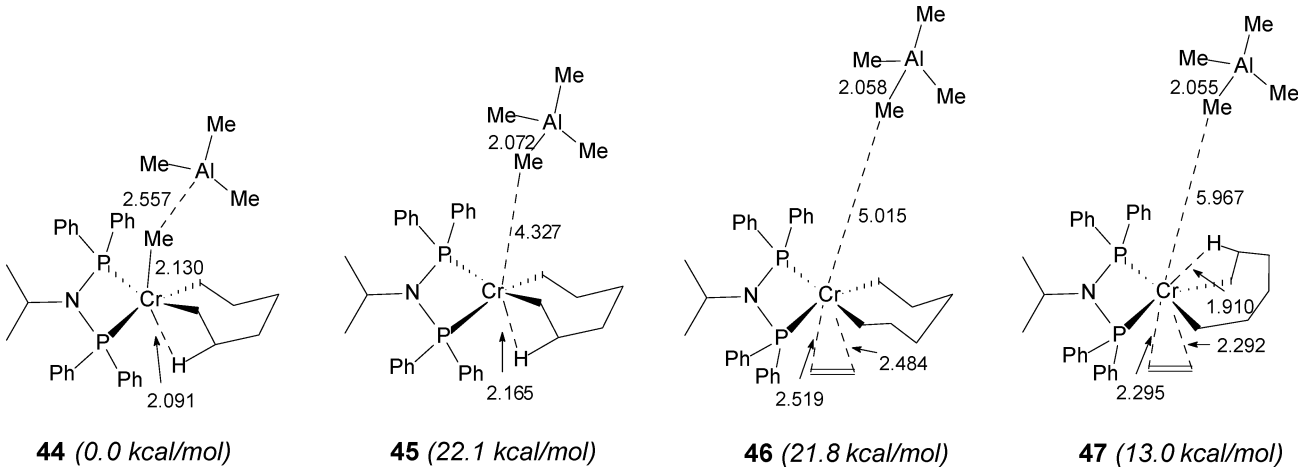

44 *(0.0 kcal/mol)* **45** *(22.1 kcal/mol)* **46** *(21.8 kcal/mol)* **47** *(13.0 kcal/mol)*

Figure 15. DMol^3/RPBE-optimized geometries for interaction of TMA with both "unsaturated" and "saturated" PNP−Ph chromacycloheptane complexes. Comparative ΔE_{ZPE} energies (kcal/mol) are presented relative to **44** and balanced with the energy of free ethylene where necessary.

$(AlOMe)_9$, and three TMA-expanded MAO cages, $(AlOMe)_6$−TMA, $(AlOMe)_9$−TMA-*sh*, and $(AlOMe)_9$−TMA-*ss*, are evaluated.

A computational comparison of the methylating aptitudes of various MAO models with the methylating aptitude of TMA dimer shows that the formation of Cr−Me species is likely to be attributed to TMA rather than MAO. Furthermore, in agreement with previous theoretical studies reported on the nature of MAO it is found that the activation of a "classic" MAO cage structure by TMA not only is energetically favorable but also results in the formation of three-coordinate Al centers in the TMA-expanded MAO structure exhibiting higher Lewis acid character. This affords more favorable interaction of MAO with the chromacycloheptane complexes via bridging Me groups. From the results a distinction is thus made between the relative ability of TMA-expanded MAO models and TMA to interact and activate chromium complexes for catalysis, which is in turn correlated to the relative abilities of TMA and MAO to accommodate delocalization of negative charge upon formation of dissociated ion-pair complexes. This suggests that the presence of free TMA in MAO is likely to play a dual role, first the methylation of precursor chromium precatalysts and second the activation of MAO itself for interaction with methylated chromium species and subsequent ion-pair formation.

From the results for interaction of TMA-expanded MAO models with appropriate chromacycloheptane complexes important differences between "stripped-down" and "full" models are obtained. In particular, in all calculations employing the "stripped-down" ligand, $Me_2PN(Me)PMe_2$, in combination with the smaller TMA-expanded MAO cage, $(AlOMe)_6$−TMA, no spontaneous formation of ion-pair complexes is found. This result also holds when the steric congestion on chromium is significantly enhanced upon coordination of an additional ethylene moiety. In contrast, calculations involving the "full" $Ph_2PN(^iPr)PPh_2$ ligand and larger TMA-expanded MAO cages, $(AlOMe)_9$−TMA-*sh* and $(AlOMe)_9$−TMA-*ss*, show that while the formation of formally coordinated chromacycloheptane−MAO complexes are successfully optimized in the absence of additional ethylene, only dissociated ion-pair complexes are present when an additional ethylene moiety is introduced. These results serve to highlight the importance of using realistic models for computational studies on these systems.[56] More importantly, however, the favorable formation of dissociated ion-pair complexes, and consequent formation of more active cationic chromium complexes, is convincingly demonstrated to be a prerequisite for catalysis to proceed.

From this study important insight is gained on the nature of MAO itself and the possible roles played by MAO during the selective oligomerization of ethylene by chromium complexes within an established metallacycle mechanistic sequence. This provides direction for the continuation of computational studies into the fundamentals of the mechanism for chromium-catalyzed ethylene tetramerization, the results of which will be reported in due course.

Acknowledgment. We thank the Sasol Olefin Transformation and Sasol Organic Synthesis Groups, in particular Johntho Dixon, Matthew Overett, Kevin Blann, and Dave Morgan, for valuable discussions, Mr. Ivan Bester (Information Management, Sasol) for infrastructure support to the Sasol Molecular Modeling Group, and Sasol Technology Research and Development for permission to publish this work.

Supporting Information Available: Chromium spin state analysis and validation results and Cartesian coordinates for optimized geometries. This information is available free of charge via the Internet at http://pubs.acs.org.

OM060890C